SUBMITTED: JUNE 21, 2018
Preprint typeset using LaTeX style emulateapj v. 12/16/11

AN EXCESS OF JUPITER ANALOGS IN SUPER-EARTH SYSTEMS

MARTA L. BRYAN[1], HEATHER A. KNUTSON[2], BJ FULTON[1,3], EVE J. LEE[4], KONSTANTIN BATYGIN[2], HENRY NGO[5], TIFFANY MESHKAT[1]

SUBMITTED: *June 21, 2018*

ABSTRACT

We use radial velocity observations to search for massive, long-period gas giant companions in systems hosting inner super-Earth ($1-4$ $R_\oplus$, $1-10$ $M_\oplus$) planets in order to constrain formation and migration scenarios for this population. We consistently re-fit all published radial velocity datasets for a sample of 65 stars and find 9 systems with statistically significant trends indicating the presence of an outer companion. We combine these radial velocity data with AO images in order to constrain the allowed masses and semi-major axes of these companions. We quantify our sensitivity to the presence of long period companions by fitting the sample with a power law distribution and find an estimated occurrence rate of $39\pm7\%$ for companions between $0.5-20$ $M_{\rm Jup}$ and $1-20$ AU. Half of our systems were discovered by the transit method and the other half were discovered by the RV method. While differences in RV baselines and number of data points between the two samples lead to different sensitivities to distant companions, we find that the occurrence rates of gas giant companions in each sample is consistent at the 0.5σ level. We compare the frequency of Jupiter analogs in these systems to the equivalent rate from field star surveys and find that Jupiter analogues are more common around stars hosting super-Earths. We conclude that the presence of outer gas giant planets does not suppress the formation of inner super-Earths, and that these two populations of planets instead appear to be correlated with each other. We also find that the stellar metallicities of systems with gas giant companions are significantly higher than those without companions, in good agreement with the well-established metallicity correlation from RV surveys of field stars.

Keywords: planetary systems – techniques: radial velocity – methods: statistical

1. INTRODUCTION

The presence or absence of outer gas giant planets can significantly influence the formation and evolution of planets on interior orbits. In our own solar system, Jupiter is thought to have played a key role in dynamically re-shaping the outer solar system architecture after the dissipation of the gas disk (Tsiganis et al. 2005), driving volatile-rich planetesimals from beyond the ice line onto shorter-period orbits (Raymond 2006; O'Brien et al. 2006; Morbidelli et al. 2012; Raymond and Izidoro 2017). At earlier times, the gap in the gas disk created by Jupiter's presence would also have suppressed the flow of solid materials into the inner disk where the terrestrial planets subsequently formed, affecting both the surface density of solids in the inner disk and also the compositions of those solids (Morbidelli and Crida 2007; Morbidelli et al. 2012; Lambrechts et al. 2014; Morbidelli et al. 2016; Desch et al. 2017). It has even been theorized that an in-and-then-out-again migration by Jupiter and Saturn (Walsh et al. 2011) might have disrupted planet formation in the inner several AU, therefore explaining why the solar system only hosts relatively small planets between $0.3-2$ AU and none interior to that (Batygin and Laughlin 2015).

Given the dominant role that gas giant planets played in the early history of the solar system, it is natural to consider their possible influence in exoplanetary systems. Broadly speaking, there are several mechanisms by which outer gas giant planets can influence the formation and evolution of interior planets. Giant planets comparable to or larger than Saturn will open a gap in the gas disk (Lin and Papaloizou 1986; Crida et al. 2006; Kley and Nelson 2012), potentially suppressing the flow of small solids ("pebbles") to the inner disk. Moriarty and Fischer (2015) find that the rate of planetesimal growth in the inner disk is sensitive to the rate at which pebbles drift radially inward, implying that systems with giant planets should have fewer and less massive planets in the inner region of the disk. However, the presence of a giant planet will also create local pressure maxima that collect solids, potentially sparking a secondary wave of planet formation (Whipple 1972; Masset et al. 2006; Rice et al. 2006; Hasegawa and Pudritz 2011; Morbidelli and Nesvorny 2012; Sato et al. 2016).

Through resonant transport associated with migration, gas giants can also dynamically excite the population of planetesimals from which rocky planets are forming, increasing the likelihood that collisions will result in disruption rather than accretion (Walsh et al. 2011; Batygin and Laughlin 2015). However, unless this disrupted material is subsequently accreted onto the host star, this dynamical excitation and disruption of material is not a barrier to rocky planet formation (Wallace et al. 2017).

[1] Cahill Center for Astronomy and Astrophysics, California Institute of Technology, 1200 East California Boulevard, MC 249-17, Pasadena, CA 91125, USA
[2] Division of Geological and Planetary Sciences, California Institute of Technology, Pasadena, CA 91125 USA
[3] IPAC-NASA Exoplanet Science Institute, Pasadena, CA 91125 USA
[4] TAPIR, Walter Burke Institute for Theoretical Physics, Mailcode 350-17, California Institute of Technology, Pasadena, CA 91125, USA
[5] National Research Council of Canada, Herzberg Astronomy and Astrophysics, 5071 West Saanich Road, Victoria, BC, V9E 2E7, Canada

Dynamically hot outer gas giants can perturb inner planets onto eccentric and/or inclined orbits, reducing the multiplicity of planets in those systems (Hansen 2017; Pu and Lai 2018) or leading to orbital instability within a few Myrs in some extreme cases (Huang et al. 2017). These same gas giants can also act as a barrier that prevents smaller planets formed in the outer disk (i.e., beyond the orbit of the gas giants) from migrating inward (Izidoro et al. 2015).

Even if they do not directly influence the formation or dynamical evolution of inner planetary systems, the presence of an outer gas giant planet is in and of itself a statement about the properties of the primordial disk. In the core accretion model (Pollack et al. 1996), cores must form before the disk gas dissipates in order to acquire massive envelopes. The well-established correlation between gas giant planet frequency and stellar metallicity for sun-like stars (Fischer and Valenti 2005; Johnson et al. 2010) indicates that the core formation process occurs more readily in metal-rich disks (e.g. Dawson et al. 2015). The longer lifetime of disks around metal-rich stars also facilitates the formation of both gas giant planets (e.g. Yasui et al. 2010; Ercolano and Clarke 2010) and those at lower masses (e.g. Buchhave et al. 2014; Petigura et al. 2018)

Despite the relative richness of theoretical work in this area, we currently have very few observational constraints on the role that outer gas giant planets play in determining the properties of inner planetary systems. This is largely due to the limited baselines of current surveys: both transit and radial velocity (RV) surveys typically require the observation of one or more complete orbits in order to count a given signal as a secure detection, but even the longest-running surveys have baselines that are shorter than the orbital periods of the solar system gas giants (Cumming et al. 2008; Howard et al. 2010; Mayor et al. 2011; Dressing and Charbonneau 2015; Bryan et al. 2016; Rowan et al. 2016; Wittenmyer et al. 2016). Recently, several RV surveys (Wittenmyer et al. 2016; Rowan et al. 2016) estimated the frequency of Jupiter analogs, which they defined as 0.3 - 13 M_{Jup} and 3 - 7 AU (Wittenmyer et al. 2016) and 0.3 - 3 M_{Jup} and 3 - 6 AU (Rowan et al. 2016), taking into account survey incompleteness at larger separations and smaller masses. Both surveys found the frequency of Jupiter analogs to be small; Wittenmyer et al. (2016) found an occurrence rate of $6.2^{+2.8}_{-1.6}$%, while Rowan et al. (2016) found an occurrence rate of $\sim$3%. However, neither of these surveys extended as far as Saturn's orbit, and relatively few of the stars in these two samples have known inner planets. Of the super-Earth systems examined in this study, we find that only three were included in the Wittenmyer et al. (2016) sample, while Rowan et al. (2016) did not provide an explicit list of the stars included in their survey.

If we are willing to consider planet candidates with partially observed orbits, we can extend the statistical reach of these surveys to larger orbital separations. This also allows us to consider systems with inner transiting planets, which typically have shorter photometric and radial velocity baselines (on the order of 1-5 years) (e.g. Marcy et al. 2014; Weiss and Marcy 2014; Dressing et al. 2015; Astudillo-Defru et al. 2017). While the Kepler mission is in principle sensitive to transiting gas giant planets in Jupiter-like orbits (Uehara et al. 2016; Foreman-Mackey et al. 2016), the transit probability for these planets is extremely low and a majority of the long period planet candidates reported to date do not have inner transiting companions. Alternatively, long-term radial velocity monitoring of systems with known inner planets can provide information on the frequency of outer companions regardless of whether or not they transit their host stars (e.g. Montet et al. 2014; Knutson et al. 2014; Bryan et al. 2016). Although our knowledge of the masses and orbital periods of these objects are incomplete, we can nonetheless search for correlations between inner planet properties and the presence or absence of an outer companion.

In previous studies we considered the frequency of outer companions in systems with transiting hot Jupiters (Knutson et al. 2014) and with inner gas giant planets spanning a range of orbital periods (Bryan et al. 2016). In this study we focus on stars known to host one or more super-Earth planets (defined as $1-4$ $R_\oplus$ or $1-10$ $M_\oplus$, depending on the detection method) located inside 0.5 AU. These planets dominate the observed population of planets orbiting nearby stars, with 30-50% of Sun-like stars hosting one or more super-Earths with orbital periods less than 100 days (Howard et al. 2010; Fressin et al. 2013; Petigura et al. 2013; Zhu et al. 2018). We identify published RV data for a sample of 65 systems hosting inner super-Earths and use these data to search for long-period gas giant companions. In section 2 we describe our sample of systems. In section 3 we describe our fits to the RV data, identification of non-planetary sources of RV trends, our calculation of companion probability distributions, and our completeness estimations. Finally, in section 4 we discuss the occurrence rate of gas giant companions in our sample and implications of our results.

2. OBSERVATIONS

We collected published radial velocity (RV) data for systems with at least one confirmed super-Earth, where we define a super-Earth as a planet with either a mass between $1-10$ $M_\oplus$ or a radius between $1-4$ $R_\oplus$, depending on the detection technique (Table 1). We exclude systems with fewer than ten data points and baselines shorter than 100 days, leaving us with 65 systems that meet these criteria (Figure 1). Of that sample, 34 systems host at least one super-Earth discovered using the transit method, and 31 systems host at least one super-Earth discovered using the RV method. 18 of these systems are single-planet systems, while the remaining 47 are multi-planet systems. 45 planets have both measured masses and radii, and thus measured densities. We provide a summary of the RV data used in this work in Table 1. We also include best-fit values for the RV acceleration from our orbital solution fitting as described in the following section.

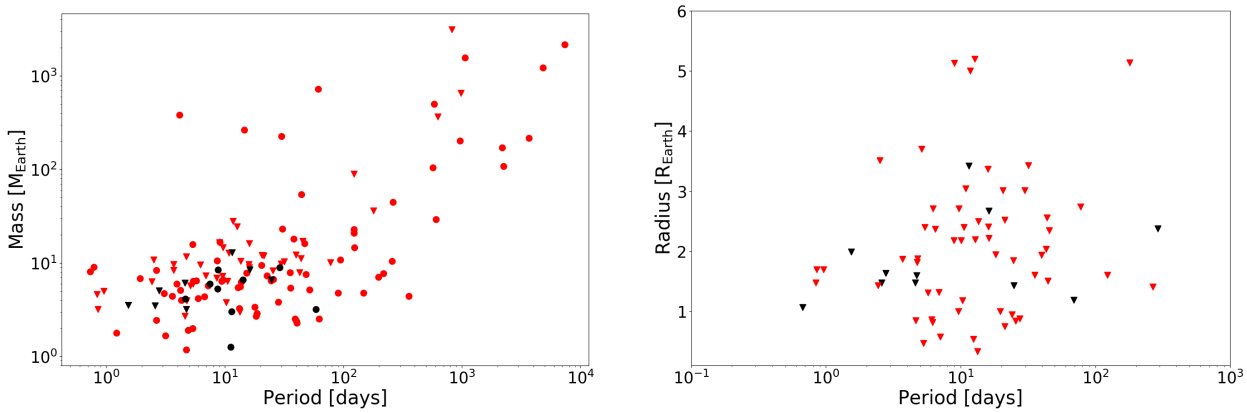

Figure 1. Confirmed planets on fully resolved orbits from our sample of 65 super-Earth hosting systems. Each system contains at least one super-Earth ($1-4$ R$_\oplus$, $1-10$ M$_\oplus$), but some also host well-characterized outer planets with larger masses and radii. We show the planets with measured masses as a function of period on the left, and planets with measured radii on the right. Systems discovered using the transit method are shown as filled triangles, while systems discovered by the RV method are shown as filled circles. Planets in multi-planet systems are plotted in red, while single planets are plotted in black.

Table 1
Sample of systems

Target	M$_\star$ (M$_\odot$)	[Fe/H][1]	N$_{pl}$	Disc. Method	N$_{obs}$	Baseline (days)	Trend (m s^{-1} yr^{-1})	Ref.
Kepler-93	0.91±0.03	-0.09±0.04	1	Transit	118	1892	**12.01±0.44**	1,2,48
Kepler-95	1.08±0.08	0.27±0.04	1	Transit	31	1078	$0.62^{+1.17}_{-1.13}$	2,48
Kepler-96	1.00±0.06	0.10±0.04	1	Transit	26	772	$-1.50^{+1.17}_{-1.10}$	2,48
Kepler-97	0.94±0.06	-0.16±0.04	1	Transit	20	789	$\mathbf{-4.49}^{+1.31}_{-1.35}$	2
Kepler-98	0.99±0.06	0.20±0.04	1	Transit	22	805	$2.34^{+2.15}_{-2.04}$	2,48
Kepler-99	0.79±0.06	0.18±0.04	1	Transit	21	792	$-2.96^{+1.35}_{-1.39}$	2,48
Kepler-21	$1.41^{+0.02}_{-0.03}$	-0.04±0.04	1	Transit	122	1756	0.73 ± 1.05	3,4,48
Kepler-22	0.97±0.06	-0.20±0.04	1	Transit	16	373	$0.84^{+3.13}_{-3.32}$	5,48
Kepler-407	1.00±0.06	0.41±0.04	1	Transit	17	750	**-156.59** ± 4.02	2,48
LHS 1140	0.15±0.02	-0.24±0.10	1	Transit	144	386	0.44 ± 1.68	6
Kepler-409	0.92±0.06	0.12±0.04	1	Transit	25	175	8.76 ± 6.21	2,48
Kepler-94	0.81±0.06	0.32±0.04	2	Transit	29	799	$28.11^{+18.62}_{-20.44}$	2,48
Kepler-103	1.09±0.07	0.13±0.04	2	Transit	19	736	2.70 ± 1.79	2,48
Kepler-109	1.04±0.06	-0.02±0.04	2	Transit	15	1092	$-2.59^{+2.48}_{-2.81}$	2,48
Kepler-113	0.75±0.06	0.13±0.04	2	Transit	24	833	0.15 ± 3.65	2,48
Kepler-131	1.02±0.06	0.19±0.04	2	Transit	20	742	$0.073^{+2.11}_{-2.19}$	2,48
Kepler-406	1.07±0.06	0.28±0.04	2	Transit	42	801	0.73 ± 1.10	2,48
Kepler-10	0.91±0.02	-0.11±0.04	2	Transit	148	510	$3.72^{+2.04}_{-1.97}$	8,48
Corot-7	0.93±0.03	0.03±0.06	2	Transit	109	357	10.95 ± 7.30	9,49
Corot-24	0.91±0.09	0.30±0.15	2	Transit	50	1154	**-10.95 ± 2.92**	10
Kepler-454	$1.03^{+0.04}_{-0.03}$	0.28±0.04	2	Transit	102	1901	$\mathbf{14.56}^{+0.58}_{-0.62}$	11,48
Kepler-100	1.08±0.06	0.10±0.04	3	Transit	49	1221	1.06 ± 0.80	2,48
Kepler-25	1.19±0.06	-0.05±0.04	3	Transit	62	828	$2.23^{+2.41}_{-2.30}$	2,48
Kepler-37	0.80±0.07	-0.25±0.04	3	Transit	33	862	0.26 ± 1.06	2,48
Kepler-68	1.08±0.05	0.14±.04	3	Transit	64	1207	$1.68^{+0.77}_{0.803}$	2,48
K2-3	0.61±0.09	-0.32±0.13	3	Transit	72	103	$10.95^{+6.94}_{-7.67}$	12
Kepler-20	0.91±0.03	0.11±0.04	6	Transit	30	650	$-1.61^{+2.48}_{-2.56}$	13,48
K2-32	0.86±0.03	0.43±0.04	3	Transit	74	441	$2.41^{+2.04}_{-2.01}$	14
Kepler-106	1.00±0.06	-0.09±0.04	4	Transit	25	1074	-0.96 ± 1.3	2,48
Kepler-48	0.88±0.06	0.26±0.04	4	Transit	28	1135	$2.01^{+3.10}_{-3.32}$	2,48
Kepler-102	0.81±0.06	0.11±0.04	5	Transit	35	897	$1.06^{+1.13}_{-1.10}$	2,48
Kepler-62	0.69±0.02	-0.34±0.04	5	Transit	13	128	$60.2^{+42.0}_{-32.0}$	15,48
55 Cnc	0.94±0.05	0.31±0.04	5	RV	663	8476	$-0.33^{+0.16}_{-0.15}$	16,17,56
61 Vir	$0.95^{+0.04}_{-0.03}$	-0.01±0.10	3	RV	786	7060	-0.31 ± 0.14	18, 19,56
GJ 15A	0.38±0.06	-0.32±0.17	1	RV	349	6215	$-0.44^{+0.077}_{-0.073}$	19, 20
GJ 176	0.50	0.15±0.17	1	RV	167	5836	$-0.27^{+0.34}_{-0.35}$	19,21,53
GJ 273	0.29	-0.17±0.17	2	RV	354	6855	$\mathbf{1.2}^{+0.066}_{-0.062}$	19, 22, 53
GJ 433	0.48	-0.22±0.10	1	RV	100	5476	$-0.22^{+0.22}_{-0.20}$	19,23
GJ 536	0.52±0.05	-0.08±0.09	1	RV	228	6128	-0.13 ± 0.10	19, 24
GJ 581	0.31±0.02	-0.10±0.17	3	RV	531	5139	$0.43^{+0.16}_{-0.15}$	19,25,53
GJ 667 C	0.33±0.02	-0.59±0.10	5	RV	238	4847	**1.79 ± 0.18**	19,26,27,54
GJ 3341	0.47	-0.09±0.09	1	RV	135	1456	0.27± 0.20	28
HD 215497	0.87±0.02	0.23±0.07	2	RV	99	1842	-0.24 ± 0.23	29

Table 1 — *Continued*

Target	$M_\star$ ($M_\odot$)	[Fe/H][1]	N_{pl}	Disc. Method	N_{obs}	Baseline (days)	Trend (m s^{-1} yr^{-1})	Ref.
HD 156668	0.77±0.02	0.05±0.06	1	RV	527	4226	-0.15 ± 0.12	30,52
HD 20794	0.70	-0.40±0.01	4	RV	187	2610	$-0.044^{+0.047}_{-0.044}$	31
GJ 832	0.45±0.05	-0.30±0.20	2	RV	109	5569	$0.14^{+0.21}_{-0.22}$	32
HD 181433	0.78	0.33±0.13	3	RV	107	1757	$1.5^{+0.98}_{-2.9}$	33
HD 7924	$0.83^{+0.02}_{-0.04}$	-0.15±0.03	3	RV	906	4783	0.080 ± 0.051	34
GJ 3138	0.68	-0.30±0.12	3	RV	199	2932	$0.20^{+0.12}_{-0.13}$	22
GJ 3323	0.16	-0.06±0.17	2	RV	142	4333	0.12 ± 0.11	22,53
HD 1461	1.02	0.19±0.01	2	RV	921	6310	$-0.055^{+0.16}_{-0.15}$	19, 35
Proxima Cen	0.12±0.02	0.22±0.03	1	RV	144	4325	$-0.13^{+0.10}_{-0.095}$	36,51,55
HD 3167	0.86±0.03	0.04±0.05	3	Transit	251	152	$\mathbf{9.96}^{+1.97}_{-2.04}$	37
GJ 3998	0.50±0.05	-0.16±0.09	2	RV	136	869	$-0.66^{+0.55}_{-0.51}$	38
GJ 876	0.33±0.03	0.19±0.17	4	RV	389	6074	0.69 ± 0.38	19,39,53,56
GJ 3293	0.42	0.02±0.09	4	RV	205	2311	-0.11 ± 0.11	22
HD 40307	0.77	-0.31±0.03	5	RV	226	3811	0.55 ± 0.040	35
HD 175607	0.74±0.05	-0.62±0.01	1	RV	110	3390	$0.13^{+0.11}_{-0.12}$	40
GJ 163	0.40±0.04	-0.01±0.10	3	RV	153	3068	-0.12 ±0.16	41
HD 219134	0.81±0.02	0.11±0.04	6	RV	992	4096	-0.66 ± 0.084	19,42,56
GJ 3634	0.45±0.05	-0.10±0.10	1	RV	54	460	$9.6^{+0.95}_{-1.0}$	43
HD 85512	0.69	-0.33±0.03	1	RV	185	2745	0.32 ± 0.051	31
GJ 676	0.71±0.04	0.23±0.10	3	RV	127	3231	$\mathbf{0}$ ± $\mathbf{0}$[2]	44
WASP-47	0.99±0.05	0.36±0.05	4	Transit	146	2340	$-1.31^{+1.28}_{-2.26}$	45, 46, 47
Wolf 1061	0.29	-0.02±0.17	3	RV	187	4136	$0.037^{+0.058}_{-0.055}$	22,53

Note. — References: (1) Dressing et al. (2015), (2) Marcy et al. (2014), (3) López-Morales et al. (2016), (4) Howell et al. (2012), (5) Borucki et al. (2012), (6) Dittmann et al. (2017), (7) Berta-Thompson et al. (2015), (8) Dumusque et al. (2014), (9) Queloz et al. (2009), (10) Alonso et al. (2014), (11) Gettel et al. (2016), (12) Almenara et al. (2015), (13) Gautier et al. (2012), (14) Petigura et al. (2017a), (15) Borucki et al. (2013), (16) Endl et al. (2012), (17) Nelson et al. (2014), (18) Vogt et al. (2010), (19) Butler et al. (2017), (20) Howard et al. (2014), (21) Forveille et al. (2009), (22) Astudillo-Defru et al. (2017), (23) Delfosse et al. (2013), (24) Suárez Mascareño et al. (2017), (25) Mayor et al. (2009), (26) Anglada-Escudé et al. (2013), (27) Anglada-Escudé et al. (2012), (28) Astudillo-Defru et al. (2015), (29) Lo Curto et al. (2010), (30) Bryan et al. (2016), (31) Pepe et al. (2011), (32) Wittenmyer et al. (2014), (33) Bouchy et al. (2009), (34) Fulton et al. (2015), (35) Diaz et al. (2016), (36) Anglada-Escudé et al. (2016), (37) Christiansen et al. (2017), (38) Affer et al. (2016), (39) Correia et al. (2010), (40) Mortier et al. (2016), (41) Bonfils et al. (2013), (42) Gillon et al. (2017), (43) Bonfils et al. (2011), (44) Sahlmann et al. (2016), (45) Sinukoff et al. (2017), (46) Neveu-VanMalle et al. (2016), (47) Dai et al. (2015), (48) Petigura et al. (2017b), (49) Léger et al. (2009), (50) Bonfils et al. (2005), (51) Schlaufman and Laughlin (2010), (52) Howard et al. (2011), (53) Rojas-Ayala et al. (2012), (54) Cayrel de Strobel et al. (2001), (55) Zhao et al. (2018), (56) Fischer et al. (2014).

[1] We note that uncertainties on the metallicity were not published for systems 61 Vir, GJ 433, GJ 667, Proxima Cen, and GJ 3634. For these systems we adopt metallicity uncertainties of 0.1 dex.

[2] Because the RV acceleration in GJ 676 has curvature, we fit this long period signal with an orbital solution. Since this partially resolved orbit and a linear trend are degenerate, we fix the linear trend term in this fit to zero, as well as the eccentricity of this outer companion.

3. ANALYSIS

3.1. *RV Fitting*

The presence of a distant companion manifests as a long term trend in the RV data when the orbital period of the companion is significantly longer than the RV baseline. In order to quantify the significance of these long-term trends, we simultaneously fit for the orbits of the known inner planets as well as a linear trend in each dataset using RadVel (Fulton et al. 2018). After identifying the best-fit solution for each data set, we next carry out a Markov Chain Monte Carlo (MCMC) exploration of the parameter space to determine the uncertainties on each model parameter. For a system with a single known planet, our model has eight free parameters including six orbital parameters (the planet's velocity semi-amplitude, orbital period, eccentricity, argument of periastron, true anomaly, and an RV zero point), a linear velocity trend, and stellar jitter.

We fit using the basis $[P, T_c, \sqrt{e}\sin\omega, \sqrt{e}\cos\omega, K]$ and impose flat priors on all of these orbital elements. For the planets that transit, we apply Gaussian priors centered on the orbital period and time of conjunction values derived from the transit data with a width equal to the measured uncertainties on these values. In cases where we include data from multiple telescopes or where the HIRES data include observations taken prior to the 2004 detector upgrade (Vogt et al. 2005; Bryan et al. 2016), we fit a separate RV zero point and jitter value for each dataset. We do not include datasets that have fewer than 10 data points. We also bin each set of radial velocity data in two-hour increments, binning datasets from different telescopes separately. We define our likelihood function in Equation 1, where σ_i is the instrumental error, σ_{jit} is the stellar jitter, v are the data, and m is the model.

$$\mathscr{L} = \prod_i \frac{1}{\sqrt{2\pi}\sqrt{\sigma_i^2+\sigma_{jit}^2}} \exp\left(-0.5\left(\frac{(v_i-m_i)^2}{\sigma_i^2+\sigma_{jit}^2}\right)\right) \quad (1)$$

We initialize each MCMC chain using the best-fit parameters from our fit. We note that for several systems we fit a different number of Keplerian orbits than the published number of planets (Table 1). Of the transiting planet systems, this includes Kepler-20 and Kepler-407. For Kepler-20 there are six published planets but we fit three Keplerian orbits, as three of the transiting planets did not yield statistically significant RV semi-amplitudes in previous studies (Gautier et al. 2012). For Kepler-407, there is one transiting planet and a long-term trend with

curvature that was published as a planet detection, but we only fit a full Keplerian orbit for the inner planet as the outer planet's orbital period is poorly constrained by the current RV data (Marcy et al. 2014).

For the RV-detected planetary systems, we search for periodic signals in the radial velocity datasets using the automated planet search pipeline described in Fulton et al. (2015). We fit Keplerian orbits to all signals with empirical false alarm probabilities (eFAP) less than or equal to 1% and K greater than or equal to 1.0 m/s in our final RV analysis. For systems GJ 667, GJ 876, and HD 40307, we find that we are only able to recover a subset of the previously published planets, and fit for 3, 3, and 4 planetary orbits, respectively in these systems.

For GJ 3341, HD 156668, HD 175607, and GJ 163 we find additional periodic signals with eFAP$\leq$1% that do not correspond to the periods of the confirmed planets in these systems and may be due to either stellar activity or additional unconfirmed planetary companions. We determine whether to include these additional periodic signals by comparing model fits with and without these additional signals using the Bayesian Information Criterion (BIC). The BIC is defined as: BIC $= -2L + k \ln n$, where L is the log likelihood of a model fit, k is the number of free parameters in the model, and n is the number of data points. In this case, the preferred model is the one with the lowest BIC value. If the BIC value for the model with additional periodic signals is smaller than the BIC value for the model without the additional periodic signals by at least 10 (a reasonable rule of thumb for statistically significant improvements in fit; Kass and Raftery 1995), we consider the model with additional period signals to be a better fit, and include these signals in subsequent analyses.

For GJ 3341, using the automated planet search pipeline we recover the known 14.2 day period planet and also detect a second signal with a period of 202 days and an amplitude of 2.0 m/s (eFAP = 1%). When we compare BIC values between model fits to the RV data with and without this 202 day signal, we find that the BIC value for the model with the additional periodic signal is only slightly smaller than the BIC value for the model without the additional periodic signal (ΔBIC= 3.9). We therefore do not include this additional periodic signal in the RV model fits to the data.

For HD 156668, the known planet with a period of 4.6 days is easily detected by our automated pipeline. We also detect a second signal at a period of 808 days with an amplitude of 2.9 m/s and a very low false alarm probability. This appears to be a promising planet candidate but will require additional vetting in order to assess its planetary nature. When comparing model fits, we find that ΔBIC = 99.9 between the model without the additional signal and the model with the additional signal, and thus include this 808 day signal in our RV model fits. If real, this signal would correspond to a planet with $M \sin i = 31$ M$_\oplus$.

For HD 175607, which has a known planet with an orbital period of 29 days, we detect a second signal with an eFAP of 0.5% and a period of 707 days. However, this period is very close to two years and has poor phase coverage as a result. We also see a third peak in the periodigram at double this period ($\sim$1400 days), indicating that there is some ambiguity in the true period of this signal. When comparing model fits, we find that ΔBIC = 27.4 between the model without the additional signal and the model with the additional signal, and thus include this 707 day signal in our RV model fits. We note however that this additional signal will likely require additional RV observations to confirm or disprove its planetary nature. If real, this signal would correspond to a planet with $M \sin i = 24$ M$_\oplus$.

Finally, for GJ 163 we detect signals corresponding to the three previously confirmed planets as well as two additional signals at periods of 19 and 108 days. Bonfils et al. (2013) previously identified these two signals as potential planet candidates. We find that a model including these additional signals is a significantly better fit to the RV data than a model that does not include these signals (ΔBIC = 12.1), so we include all five signals in our RV analysis.

After fitting our model to each data set, we search for systems with statistically significant linear trends (defined here as fits where the linear slope differs from zero by more than 3σ). We list the best-fit trend values from the maximum-likelihood fit for each system in Table 1, with corresponding uncertainties determined from the MCMC chains. We find that 14 of the 65 systems in our sample have statistically significant trends. We used the BIC to determine whether these statistically significant long term trends were best modeled with a linear trend, a quadratic trend, or an additional Keplerian orbit. In all cases but one (GJ 676) we found that a linear trend was the preferred model. For GJ 676, the curvature of the trend was significant enough to justify a fit with a full Keplerian orbital model.

We also find nine systems in our sample with fully resolved outer gas giant companions that were previously identified in the published literature. For the purposes of this study, we define an outer "gas giant" as a companion with a mass greater than 0.5 M$_{\rm Jup}$ outside of 1 AU. Although some super-Earths in our sample also have outer companions with masses smaller than this cutoff, these planets were likely too small to open a gap in the protoplanetary gas disk (e.g., Lin and Papaloizou 1986; Crida et al. 2006; Kley and Nelson 2012). The 1 AU cutoff includes all gas giants >0.5 M$_{\rm Jup}$ orbiting exterior to lower mass planets, and excludes four gas giant planets orbiting at smaller separations (55 Cnc b at 0.11 AU, GJ 876 b and c at 0.21 and 0.13 AU respectively, and WASP-47 b at 0.05 AU).

We list the properties of these previously confirmed outer gas giant planets in Table 2.

Table 2
Properties of Outer Gas Giant Companions on Resolved Orbits

Companion	Mass (M$_{\rm Jup}$)	a (AU)	Ref.
Kepler 94 c	9.84±0.63	1.60±0.04	Marcy et al. (2014)
Kepler 454 c	4.46±0.12	1.29±0.02	Gettel et al. (2016)
Kepler 68 d	0.84±0.05	1.47±0.03	Marcy et al. (2014)
Kepler 48 e	2.07±0.08	1.85±0.04	Marcy et al. (2014)
55 Cnc d	3.88±0.07	5.50±0.03	Nelson et al. (2014)
GJ 832 b	0.68±0.09	3.56±0.28	Wittenmyer et al. (2014)
HD 181433 c	0.65	1.76	Bouchy et al (2009)
HD 181433 d	0.54	3.00	Bouchy et al (2009)
GJ 676 b	4.96±0.96	1.82±0.06	Stassun et al. (2017)
WASP 47 c	1.29±0.06	1.38±0.02	Sinukoff et al. (2017)

3.2. *AO Imaging*

For the systems with statistically significant trends, we obtained AO imaging data to determine whether these systems had stellar companions that might have caused the observed trend. We identified published AO images (Tanner et al. 2010; Alonso et al. 2014; Howard et al. 2014; Rodriguez et al. 2015; Sahlmann et al. 2016; Furlan et al. 2017; Ngo et al. 2017; Christiansen et al. 2017) for all but three of these systems. Of the remaining three systems, two (HD 40307 and HD 85512) had unpublished archival data obtained with the NACO instrument (Lenzen et al. 2003; Rousset et al. 2003) on the Very Large Telescope (VLT). The HD 40307 data were taken in Ks-band with a total integration time of 1.1 hr (ID: 088.C-0832(A), PI: Loehne). The HD 85512 data were obtained in Ks-band with a total integration time of 9 minutes (ID: 090.C-0125(A), PI: Mugrauer). Both datasets were obtained without a coronagraph, using a 4-point dither pattern.

We downloaded the data for both stars from the ESO archive and processed them using the pipeline outlined in Meshkat et al. (2014). We did not detect any stellar companions in either of these datasets. We show 5σ Ks contrast values for both systems in Table 3.

Table 3
5σ Contrast Curves

System	Separation (arcsec)	5σ Contrast (mag)
HD 40307	0.79	9.47
	1.90	10.87
	2.99	11.72
	4.07	11.45
	5.16	11.91
	6.24	11.90
	7.33	12.06
	8.42	12.63
	9.50	12.66
HD 85512	0.79	4.41
	1.28	6.95
	1.76	7.40
	2.25	8.06
	2.74	8.68
	3.23	9.34
	3.69	9.95
	4.18	9.44
	4.67	10.07
GJ 3634	0.09	0.014
	0.22	3.92
	0.35	4.81
	0.49	5.24
	0.63	6.18
	0.77	6.71
	0.91	6.92
	1.05	7.15
	1.18	7.11
	1.32	7.18
	1.46	7.20
	1.60	7.11
	1.74	7.14
	1.88	7.05
	2.02	7.05
	2.16	7.05
	2.30	7.10
	2.43	7.05
	2.57	7.04
	2.71	7.11
	2.85	7.05
	2.99	7.13
	3.13	7.06
	3.26	7.01

Table 3 — *Continued*

System	Separation (arcsec)	5σ Contrast (mag)

For the remaining system (GJ 3634), we obtained K_c-band AO images using NIRC2 at Keck on UT Feb 5 2018 with an effective integration time of 9 seconds and a three-point dither pattern. We identified a close pair of candidate companions at a separation of $1''.8$ and used a multi-peak point spread function (PSF) to simultaneously fit GJ 3634 and the two candidate companions in each frame where the companion is resolved. We constructed the PSF as a sum of Moffat and Gaussian functions and fit over a circular aperture of 10 pixels in radius, corresponding to twice the full width at half maximum (FWHM) of the PSF as described in Ngo et al. (2015).

We next integrated the best-fit PSFs for GJ 3634 and its candidate companions over the same aperture to determine their flux ratios. We similarly measured the companion separation and position angle by calculating the difference between the centroids of each star. We then applied the NIRC2 astrometric corrections from Service et al. (2016) to compensate for the NIRC2 array's distortion and rotation. We find that the easternmost candidate companion (labeled as cc1 in Figure 2) has a flux ratio of 116, corresponding to $\Delta K_c = 5.16$. This companion is separated from GJ 3634 by $1''.778 \pm 0''.002$ at a position angle of $177.37° \pm 0.04°$ east of north. For the western candidate companion (cc2), we measure a flux ratio of 75 ± 8, corresponding to $\Delta K_c = 4.7 \pm 0.1$. This companion is separated from GJ 3634 by $1''.860 \pm 0.''002$ at a position angle of $203.40° \pm 0.05°$ east of north. We calculate our uncertainties as the quadrature sum of measurement uncertainties and the uncertainty in the distortion solution. However, in one of the three frames cc1 did not have a regular PSF shape and as a result we were unable to fit for its peak and location. With just two independent measurements for this companion, we are unable to calculate an empirical measurement uncertainty and therefore only report the astrometric distortion solution uncertainties.

For each companion in GJ 3634, we determine stellar masses using PHOENIX spectral models and the Baraffe et al. (1998) zero age main sequence models. We first select a PHOENIX model for the primary star based on the published stellar properties and then determine the companion's effective temperature by identifying the PHOENIX model that most closely matches the observed flux ratio. For each PHOENIX model, we determine the corresponding stellar mass and radius using the Baraffe et al. models. For both companions, we find best-fit masses of 0.08 $M_\odot$. However, as we only have one epoch of data for this system, we are unable to determine whether or not these companions are bound to the primary. We note, however, that this is a high proper motion target (-582.8, -92.1 mas/yr) and astrometric measurements with just a one year baseline would easily determine whether these companions are bound.

We next consider whether or not the RV trends in these systems might plausibly be explained by the presence of a nearby stellar companion. Kepler-93, Kepler-97, Kepler-407, and GJ 3634 each have candidate stellar companions, meaning that these systems have one epoch of data

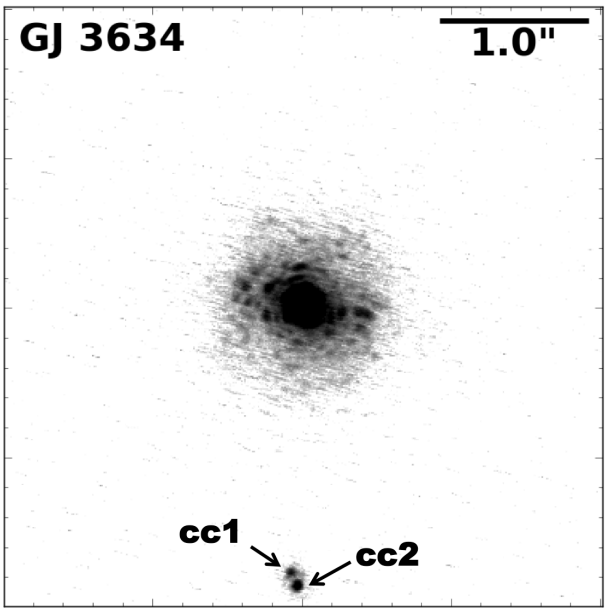

Figure 2. Reduced Keck/NIRC2 K_c-band image of GJ 3634 showing two candidate companions, labeled cc1 and cc2. Note the image is shown on a log scale, and is aligned with north towards the top and east towards the left.

showing nearby stars that could be either bound companions or distant background stars. GJ 15A and GJ 676 have confirmed stellar companions that have been shown to have the same proper motion as the primary. We calculate the minimum companion mass in each system needed to explain the observed RV trend using the equation from Torres (1999):

$$M_{\rm comp} = 5.34 \times 10^{-6} M_{\odot} \left(\frac{d}{\rm pc} \frac{\rho}{\rm arcsec} \right)^2 \times \left| \frac{\dot{v}}{\rm ms^{-1} yr^{-1}} \right| F(i, e, \omega, \phi). \quad (2)$$

In this equation, d is the distance to the star, ρ is the projected separation of the companion and the star on the sky, $\dot{v}$ is the radial velocity trend, and $F(i, e, \omega, \phi)$ is a variable that depends on the orbital parameters of the companion that are currently unconstrained. We use a value of $\sqrt{27}/2$ for F, as discussed in Liu et al. (2002). We then compare this minimum mass to the estimated mass of the candidate companion, which we calculate using the measured brightness ratio under the assumption that the candidate companion is located at the same distance as the primary star. We discuss our results for each individual system below.

Kepler-93 is 96.7 pc away and has a candidate companion with a projected separation of 2″.29 (Furlan et al. 2017). With an RV trend of 12.0 m s^{-1} yr^{-1}, this trend corresponds to a minimum companion mass of 8.2 M$_\odot$. We estimate the mass of the candidate companion using its measured magnitude M$_{\rm K}$ = 5.35 and assuming an age of 1 Gyr. We then use the Baraffe et al. (1998) models to calculate a corresponding mass of 0.57 M$_\odot$ for this companion. This mass is significantly smaller than the minimum mass needed to explain the RV trend, and we therefore conclude that this candidate companion cannot explain the observed RV trend and keep this system in our sample.

Kepler-97 is 414 pc away and has a candidate companion with a projected separation of 0″.385 (Furlan et al. 2017). With an RV trend of 4.5 m s^{-1} yr^{-1}, this trend corresponds to a minimum companion mass of 1.58 M$_\odot$. The candidate companion in this system has a magnitude M$_{\rm K}$ = 6.28, corresponding to an estimated companion mass of 0.4 M$_\odot$ using its estimated age of 8.4 Gyr. As this is smaller than the minimum mass needed to explain the RV trend, we leave this system in our sample.

Kepler-407 is 326 pc away and has a candidate companion with a projected separation of 2″.13 (Furlan et al. 2017). With an RV trend of -155.8 m s^{-1} yr^{-1}, this trend corresponds to a minimum companion mass of 1045 M$_\odot$. Given the companion's measured magnitude of M$_{\rm K}$ = 7.0 and using its estimated age of 7.5 Gyr, the estimated companion mass is 0.3 M$_\odot$. This is several orders of magnitude smaller than would be required in order to explain the observed RV trend, and we therefore leave this system in the sample.

GJ 3634 is 19.8 pc away and has two candidate companions in what appears to be a hierarchical triple system, as discussed above. These two companions are 1″.83 away from GJ 3634 and have a mutual separation of 0.087″. The measured RV trend in this system is 9.6 m s^{-1} yr^{-1}, corresponding to a minimum companion mass of 0.018 M$_\odot$. As discussed earlier, both companions have estimated masses of 0.08 M$_\odot$, indicating that their combined mass could be responsible for the observed RV trend. We thus remove this system from our sample in subsequent analyses. We note that the RV trend in this system was previously published in Bonfils et al. (2011). Given their trend, they estimate a minimum mass of 32 M$_\oplus$ and a minimum period of 200 days. Our AO image is the first to indicate that this trend might be due to the presence of stellar/brown dwarf companions rather than a distant orbiting planet.

GJ 15A is 3.6 pc away and has a confirmed stellar companion with a projected separation of 20″.28 (Howard et al. 2014). With an RV trend of -0.44 m s^{-1} yr^{-1}, this corresponds to a minimum companion mass of 0.074 M$_\odot$. The stellar companion in this system has an absolute magnitude of M$_{\rm K}$ = 8.17, corresponding to an estimated companion mass of 0.175 M$_\odot$ for an age of 1 Gyr. As this estimated companion mass is larger than the minimum companion mass needed to account for the trend, we exclude this system from our subsequent analysis.

Finally, GJ 676 is 15.9 pc away (Gaia Collaboration et al. 2016a,b) and has a confirmed stellar companion at a separation of 47″. With an RV trend of 21.6 m s^{-1} yr^{-1}, this trend corresponds to a minimum companion mass of 167 M$_\odot$. Given an absolute magnitude of M$_{\rm K}$ = 6.9, the estimated companion mass is 0.3 M$_\odot$ assuming an age of of 1 Gyr. Since this estimated companion mass is well below the minimum mass to account for the observed RV trend, we conclude this companion could not be producing the observed trend and leave this system in our sample.

3.3. *Trends Due to Stellar Activity*

We next consider whether any of the observed trends might be due to stellar activity. We examined each sys-

tem in order to determine if the measured RV trend exhibits a correlation with the star's emission in Ca II H & K lines as quantified by either the S_{HK} index or $\log R'$ (Wright et al. 2004; Isaacson and Fischer 2010). We calculated the Spearman-Rank correlation coefficients between the RV data and this activity indicator after subtracting the orbital solutions for the confirmed inner planets. We considered a correlation coefficient with an absolute value greater than 0.3 to indicate a significant correlation. We find that systems HD 219134, HD 40307, and HD 85512 have significant correlations between stellar activity and the observed RV trend, and remove these system from our subsequent analysis. We also remove HD 1461 from our analysis, as we determined in Bryan et al. (2016) that this system has a fully resolved long period signal that is significantly correlated with stellar activity.

There were two systems with RV trends for which we were not able to obtain stellar activity data, including Corot-24 and GJ 3634. We conclude that stellar activity is unlikely to be the cause of the trend in Corot-24, as the amplitude of the observed trend is higher than would be expected for stellar activity signals. Although we cannot determine whether or not the observed RV trend in the GJ 3634 might be due to stellar activity, we have already removed this system from further analysis due to the presence of candidate stellar companions that could have caused the observed trend.

After removing systems with either stellar or potentially activity-related sources of RV trends, including HD 219134, HD 85512, HD 40307, HD 1461, GJ 15A, and GJ 3634, we are left with nine systems with statistically significant trends that can plausibly be attributed to the presence of a substellar companion. We plot the RV data for each of these systems after subtracting the orbital solutions for the confirmed inner planets in Figure 3. Trends for GJ 273 (Astudillo-Defru et al. 2017), GJ 667C (Anglada-Escudé et al. 2012), GJ 676 (Anglada-Escudé and Tuomi 2012; Sahlmann et al. 2016), Kepler-93 (Marcy et al. 2014; Dressing et al. 2015), Kepler-97 (Marcy et al. 2014), Kepler-407 (Marcy et al. 2014), and Kepler-454 (Dressing et al. 2015) were previously reported in the published literature.

3.4. *Constraints on Companion Masses and Orbital Semi-Major Axes*

We use the RV data to place constraints on the masses and semi-major axes of the long period companions in each system. The duration and shape of the RV trend places a lower limit on the companion's mass and separation, while the lack of a detection in our AO imaging data places a corresponding upper limit on these quantities. As described in Bryan et al. (2016), we calculate two-dimensional probability distributions for each companion using an equally spaced 50×50 grid in logarithmic mass (true mass, not $m \sin i$), and logarithmic semi-major axis spanning a range of 0.3 - 500 M_{Jup} and 0.5 - 500 AU. In each grid cell we inject 500 simulated companions and determine whether or not they are consistent with the RV observations as follows. We first draw a set of orbital parameters for the confirmed inner planets from the previous MCMC fits, and then subtract away this orbital solution to preserve any long-term trend signal. We then draw a mass and semi-major axis value from within the grid box from a uniform distribution in log(M) and log(a), and draw an inclination from a uniform distribution in $\cos i$. We draw our eccentricity values from a beta distribution with $a = 1.12$ and $b = 3.09$, which are derived from a fit to the population of long-period gas giant planets from RV surveys (Kipping 2013). Given a fixed semi-major axis, mass, and eccentricity for each simulated companion, we then fit for the remaining orbital parameters including time of periastron, argument of periastron, and a velocity zero point and calculate the corresponding log likelihood value of the best-fit solution.

After repeating this process five hundred times in each grid cell, we convert the resulting $50 \times 50 \times 500$ cube of log likelihood values to probabilities and marginalize over our 500 samples in each grid cell to yield a two-dimensional probability distribution in mass and semi-major axis for each system. We calculate two-dimensional probability distributions for all systems in our sample, regardless of whether or not they have statistically significant trends. The only difference between those systems with and without trends is that we use our AO imaging data to place an upper limit on the companion mass and semi-major axis in the trend systems as discussed in Bryan et al. (2016). We note that for GJ 273, as a result of its close distance (3.8 pc) and the limited angular extent of the available contrast curve, the contrast curve for this system does not provide significant constraints on the mass and separation of the companion where the probability density for the companion is large. Similarly, for Corot-24 due to the significant distance of the system (600 pc), constraints provided by the available contrast curve at smaller separations where the probability density for the companion is high are not significant.

Figure 4 shows the posterior distributions for the nine systems with 3σ trends, while Table 4 indicates the corresponding 1σ limits in mass and semi-major axis for each companion.

Table 4
Constraints on Companion Properties

Companion	Mass (M_{Jup})	Semi-major Axis (AU)
Kepler 93 c	11.3 - 51.6	9.6 - 25.9
Kepler 97 c	0.18 - 166	1.2 - 60.3
Kepler 407 c	11.4 - 51.6	3.1 - 7.3
Corot 24 d	0.27 - 401	0.5 - 186
Kepler 454 d	7.2 - 81.3	9.6 - 29.8
GJ 273 d	0.55 - 430	7.3 - 214
GJ 667 h	1.2 - 430	8.4 - 214
HD 3167 e	0.05 - 85	0.8 - 22

3.5. *Completeness Maps*

We evaluate our sensitivity to distant companions in each system by calculating the completeness as a function of mass and orbital semi-major axis after taking into account the time baseline, number of data points, and measurement errors for each dataset. As before, we start with a 50×50 grid in mass and semi-major axis evenly spaced in log space from 0.3 - 500 M_{Jup} and 0.5 - 500 AU. For each grid box we inject 500 simulated companions where we draw a mass and semi-major axis from a uniformly spaced distribution across each grid box, an eccentricity value from the β distribution, inclination from

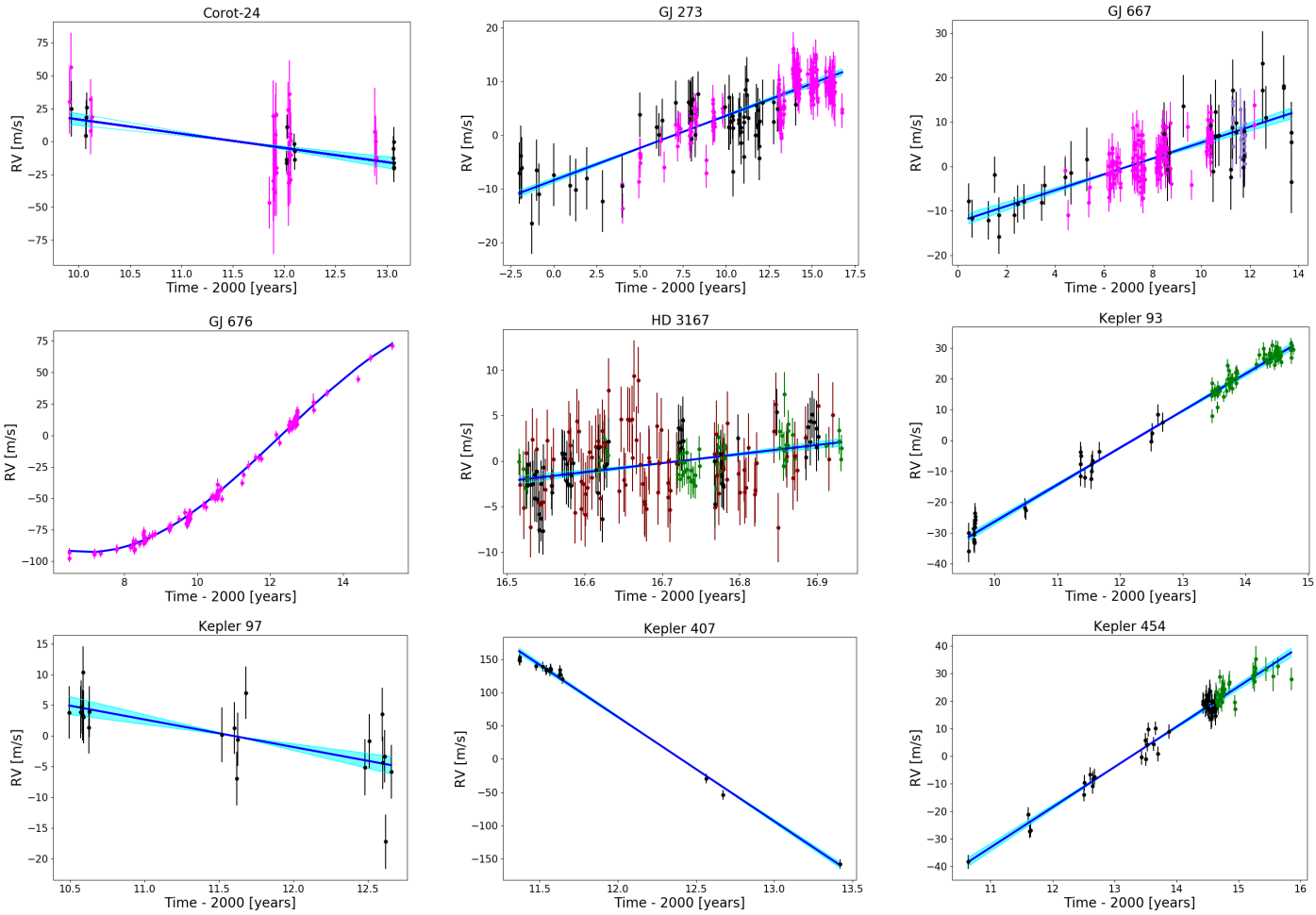

Figure 3. Best fit accelerations to the radial velocity data with a 3σ trend. The best fit trend is shown as a solid blue line, the 1σ errors on the slope are presented light blue shaded regions. The different colored data points represent RVs taken using different telescopes: black = HIRES, green = HARPS-N, pink = HARPS, light purple = PFS, maroon = APF. Note that GJ 676 has a curved trend, which allows us to place much tighter constraints on the mass and separation of the companion producing that trend.

a uniform distribution in $\cos i$, and the remaining orbital elements from uniform distributions. We then calculate the RV signal from this simulated companion at each observation epoch. We add noise into these simulated RVs by drawing from a Gaussian distribution with a width defined by $\sqrt{\sigma_i^2 + \sigma_{\rm jit}^2}$, where σ_i is the instrumental uncertainty (randomly shuffled from the original dataset) and $\sigma_{\rm jit}$ is the stellar jitter estimated from the earlier MCMC fits. To assess whether a simulated planet would be detected, we fit each simulated set of RVs with a one-planet orbital solution, a linear trend, and a flat line. We compared these model fits using the Bayesian Information Criterion (BIC) (Kass and Raftery 1995) in order to determine the simplest model that can provide an adequate fit to the data. If the BIC values for either the one-planet model fit or the linear trend were smaller than the BIC value for the flat line by at least 10, we concluded that the simulated planet would have been detected. However, if the flat line was preferred or the difference in BIC was less than 10, we counted this as a non-detection. We repeated this process for each simulated companion injected into each grid box, using our "detected/not detected" determinations to calculate the completeness over the entire grid.

Perhaps unsurprisingly, we find that the average sensitivity to companions in systems with super-Earths discovered via the transit method is significantly less than in systems with RV-detected super-Earths. This likely reflects the substantially greater investment of RV time required to detect a planet with an unknown orbital period and phase, versus the transit case where these two quantities are known precisely in advance. RV-only detections must also achieve a higher significance in their measurement of the RV semi-amplitude in order to be considered a secure detection (see representative trend system GJ 273; Forveille et al. 2009; Butler et al. 2017), whereas for RV follow-up of transiting planets even marginally significant measurements of this quantity still provide useful constraints on the planet density (see representative trend system Kepler 97; Marcy et al. 2014). We show the resulting completeness maps in Figure 5, with systems discovered using the transit method plotted separately from systems discovered using RVs in order to illustrate the different average sensitivities of these two samples.

4. DISCUSSION

4.1. *The Occurrence Rate of Gas Giant Companions*

In this section we utilize our probability distributions for each system to determine the underlying distribu-

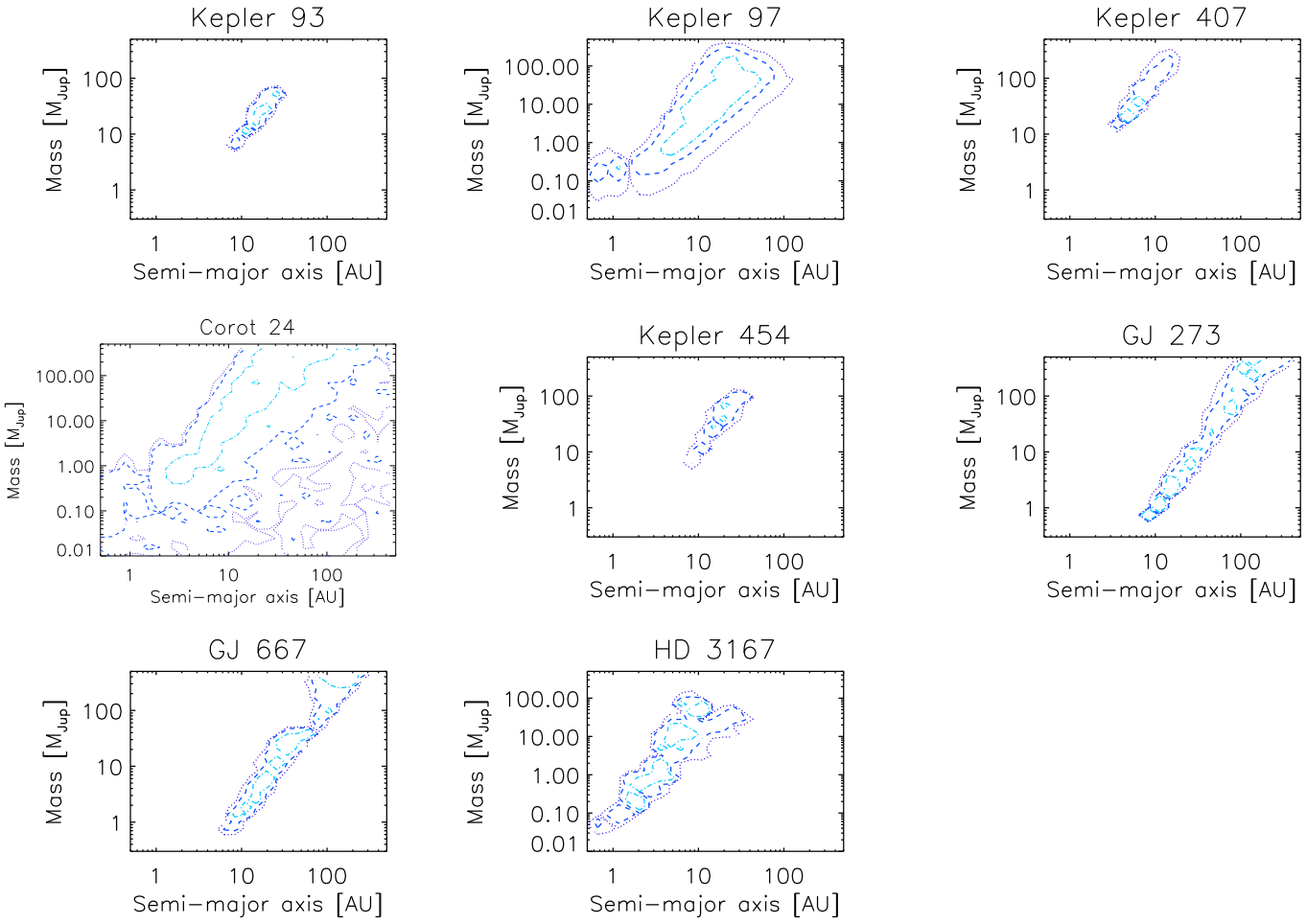

Figure 4. Probability distributions for the nine systems with statistically significant trends that are plausibly due to an orbiting substellar companion (i.e., they cannot be explained by either stellar activity or the presence of a distant stellar companion). The three contours define the 1σ, 2σ, and 3σ levels moving outward. We do not show the probability distribution for GJ 676 here, as the probability density is concentrated in just a few grid points and the contours are therefore unresolved.

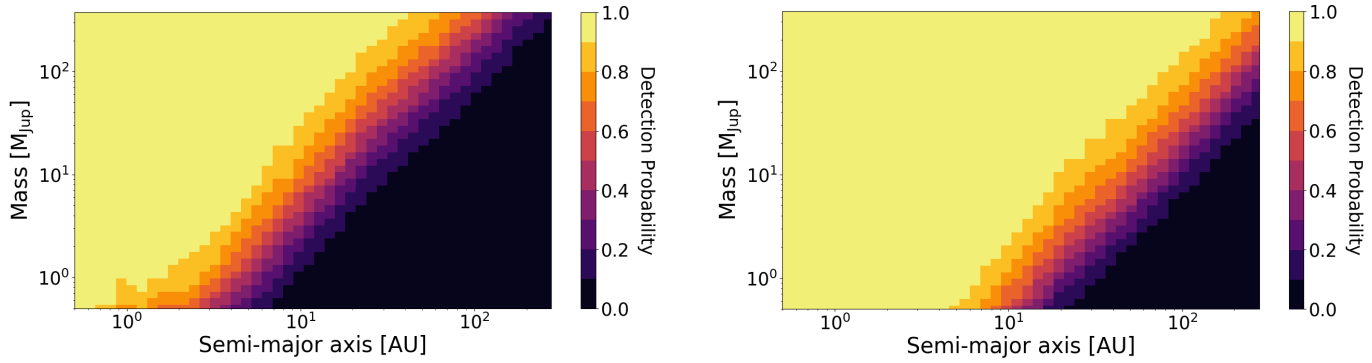

Figure 5. Sensitivity maps for the systems with super-Earths discovered using the transit method (left) and radial velocity method (right). Radial velocity detections typically require much more extensive data sets and have longer baselines than observations of transiting planet systems, resulting in different levels of completeness for these two samples.

tion and corresponding occurrence rate for the observed population of long period gas giant companions in these systems. We follow the methodology laid out in Bryan et al. (2016), and present a summary of the steps here. We first assume that this population of companions is distributed in mass and semi-major axis space according to a double power law of the form $f(m,a) = Cm^{\alpha}a^{\beta}$ (e.g. Tabachnik and Tremaine 2002; Cumming et al. 2008). The likelihood for a set of N exoplanet systems is given by:

$$\mathscr{L} = \Pi_{i=1}^{N} p(d_i|C,\alpha,\beta) \quad (3)$$

where $p(d_i|C,\alpha,\beta)$ is the probability of the RV dataset given power law coefficients C, α, and β. Assuming that each system has at most one outer companion, this likelihood is then the sum of the probability that a given system contains one planet and the probability that the system contains zero planets. The probability of a system containing zero planets is given by:

$$p(d_i,0|C,\alpha,\beta) = p(d_i|0)[1-Z] \quad (4)$$

where Z is the probability that the system contains a planet within a range of masses and semi-major axes (determined by integrating the power law distribution over the specified range), and $p(d_i|0)$ is the probability of obtaining the RV dataset given that there is no planet in the system.

The probability of a system having one companion given their distribution in mass and semi-major axis space is:

$$p(d_i,1|C,\alpha,\beta) = \int_{a_1}^{a_2} d\ln a \int_{m_1}^{m_2} d\ln m \times p(d_i|a,m)\, Cm^{\alpha}a^{\beta} \quad (5)$$

where $p(d_i|a,m)$ is the probability of a companion being located at a given mass and semi-major axis, which we know from our previously determined probability distributions (see section 3.4). To determine the likelihood of a given set of C, α, and β given our RV datasets, we combine the probabilities of a system having one planet and a system having zero planets as follows:

$$\mathscr{L} = \Pi_{i=1}^{N}\Big[p_i(d_i,0|C,\alpha,\beta) + p_i(d_i,1|C,\alpha,\beta)\Big] \quad (6)$$

As in Bryan et al. (2016), we incorporate the probability distributions for all systems in this framework, not just the distributions for systems that have statistically significant trends. This allows us to treat all systems consistently regardless of whether or not they have a statistically significant trend. Phrased another way, this allows for the possibility of marginal trend detections, rather than assuming a binary classification system in which any star with a less than 3σ trend is counted as a non-detection. For the nine systems hosting exterior gas giant (>0.5 M_{Jup}) companions on resolved orbits outside 1 AU, we replace the probability distributions calculated from the RV trends with ones where the probability density is concentrated in a single grid point closest to the best fit mass and orbital separation of the resolved companion (see Table 2 for these values).

Two of these systems (GJ 676 and Kepler-454) have both statistically significant trends and resolved gas giant companions, while HD 181433 has two resolved gas giant planet companions. In these cases, we select the innermost gas giant planet for inclusion in our power-law fit. We also note that our choice to use the inner vs outer companion in the system with more than one gas giant companion does not impact our derived power law coefficients or occurrence rates.

We determine the values of C, α, and β that maximize the value of $\mathscr{L}$ by first performing a grid search where we vary each of these power law coefficients, and then carry out a MCMC fit initialized near the location of the optimal grid point. Because these parameters are both poorly constrained and highly correlated, we find that the use of a preliminary grid search allows us to reliably identify the global maximum and reduces the convergence time in our MCMC chains.

We next use the results of these power-law fits to calculate an integrated occurrence rate for the observed population of gas giant companions over a range of masses and semi-major axes. We first calculate the integrated companion frequency separately for systems discovered using the transit method versus the radial velocity method. Given the significant differences in completeness for these two samples of systems, this allows us to evaluate the degree to which these sensitivities impact the integrated occurrence rates. We ran the grid search and MCMC analysis of each sample separately. When we calculated the occurrence rates for these two samples of systems over a mass range of 0.5 - 20 M_{Jup} and a semi-major axis range of 1 - 20 AU, we found that the occurrence rate of companions in the transiting planet sample is 41^{+10}_{-10}%, while the occurrence rate of the RV planet sample is 34^{+11}_{-10}%. These two values are consistent at the 0.5σ level. We note that the uncertainties on these occurrence rates are dominated by the number of systems in each sample, which are similar (34 for the transiting planet sample, 25 for the RV sample).

We next calculate the frequency of companions for the combined sample over different ranges in mass and semi-major axis in order to assess how occurrence rates depend on our chosen integration ranges. Table 5 shows the resulting occurrence rates for the combined sample. We note that, as in Bryan et al. (2016), the values for the power law coefficients α and β vary significantly depending on our chosen integration range as a result of the poorly constrained companion masses and separations in these systems. However, we find that we obtain consistent results for the integrated occurrence rate for these companions across a wide range of integration ranges. This is because the strongest constraint we obtain from these data is the total number of companions in these systems, while their locations are poorly constrained. As a result, we find that the preferred values for C, α, and β in our fits are correlated in a way that preserves the total number of companions regardless of the fitting range used. This stands in contrast to studies examining populations of planets with tightly constrained masses and orbital semi-major axes (e.g. Cumming et al. 2008; Bowler et al. 2010), where the values of α and β are much better constrained by the data. For these systems, we would expect the integrated occurrence rate to rise as we in-

crease the range in mass and semi-major axis, reflecting our much better knowledge of the planet occurrence rate density. This is an important point to consider when comparing our occurrence rate to those from surveys focusing on planets with fully resolved orbits, as we will discuss below.

Table 5
Total Occurrence Rates for Companions

	1 - 10 AU	1 - 20 AU	1 - 50 AU
0.5 - 20 M_{Jup}	38±7%	39±7%	41^{+8}_{-7}%
0.5 - 13 M_{Jup}	36^{+7}_{-6}%	41^{+8}_{-7}%	40^{+8}_{-7}%
1 - 20 M_{Jup}	35±7%	35±7%	38^{+8}_{-7}%
1 - 13 M_{Jup}	34±7%	38±7%	39^{+8}_{-7}%

4.2. *Comparison to Published Surveys*

We now aim to determine whether the rate of gas giant companions in super-Earth systems is higher or lower than the average occurrence rate for sun-like field stars. If there is no correlation (positive or negative) between the presence of an inner super-Earth and an outer gas giant companion, we would expect these two rates to be consistent with each other. Conversely, once we have determined the frequency of long period gas giants in super-Earth systems, we can then ask what fraction of the long period gas giants orbiting field stars are drawn from this population (i.e., what fraction of long period gas giants have inner super-Earths?). We can express this as a conditional probability:

$$p(SE|LPG) = \frac{p(LPG|SE) \times p(SE)}{p(LPG)} \quad (7)$$

where $p(SE)$ is the probability that a given star hosts a super-Earth and $p(LPG)$ is the probability of hosting a long period gas giant planet. We note that Zhu and Wu (2018) present a similar equation and provide an estimate of this probability using a sample of 32 "super-Earth" planets with masses up to 20 $M_\oplus$, approximately two thirds of which have masses between $10 - 20$ $M_\oplus$. In this study we examine 65 super-Earth-hosting stars, where we define a super-Earth as a planet having either a mass between $1 - 10$ $M_\oplus$ or a radius between $1 - 4$ $R_\oplus$ depending on the detection method. Similarly, we define a long period gas giant as a planet with a mass between $0.5 - 20$ M_{Jup} and semi-major axis between $1 - 20$ AU. When comparing to previous work we vary this definition of long-period gas giant planet to better match individual surveys as discussed below.

There have been several studies that have sought to quantify the frequency of long period gas giant planets, including Wittenmyer et al. (2016), Rowan et al. (2016), and Foreman-Mackey et al. (2016). Wittenmyer et al. (2016) calculate the occurrence rate of Jupiter analogs over the range 0.3 - 13 M_{Jup} and between 3 - 7 AU for a sample of 202 stars observed as a part of the 17-year Anglo-Australian Planet Search. For their sample of targets, they only consider planets with fully resolved orbits and find an integrated occurrence rate of $6.2^{+2.8}_{-1.6}$% over this range assuming binomial statistics (i.e., they do not fit a power law distribution). Integrating our sample over this same mass and semi-major axis range, we find an occurrence rate of 34±7%, which differs from the Wittenmyer et al. (2016) value by 3.7σ (Figure 6). We note that for this occurrence rate calculation, in a system with two gas giant companions (either both resolved or one resolved, one statistically significant trend), if the innermost resolved companion does not fall within this integration range, we use the outer companion (this was the case for systems HD 181433, GJ 676, and Kepler-454). As stated previously, the inclusion of either the closer resolved gas giant companions or the farther out signals does not affect our occurrence rate calculations over the range 0.5 - 20 M_{Jup} and 1 - 20 AU.

In order to determine whether or not the difference between our occurrence rate of 34±7% and the $6.2^{+2.8}_{-1.6}$% rate is meaningful, we must consider the possible biases introduced by our decision to consider trends rather than limit our study to companions with fully resolved orbits. Specifically, our occurrence rate is partially derived from a population of planets with probability distributions extending over a wide range of masses and semi-major axes. This means that when we integrate over the relatively narrow range used in the Wittenmyer study, our occurrence rate may be inflated by the inclusion of planets whose probability distributions overlap with this integration range, even though the planets themselves are in fact located on more distant orbits.

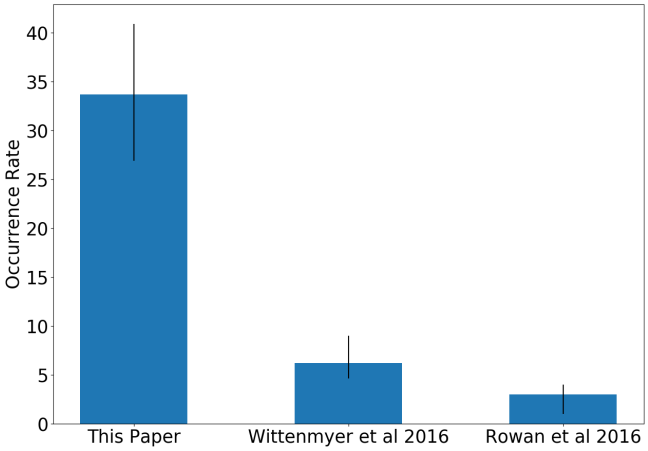

Figure 6. Compared to the Jupiter analog occurrence rate estimates published in Wittenmyer et al. (2016) and Rowan et al. (2016), this study finds a higher occurrence rate of distant gas giant planets in super-Earth systems than would be expected just based on chance. Occurrence rate integration ranges are 0.3 - 13 M_{Jup} and 3 - 7 AU for this paper and Wittenmyer et al. (2016), and 0.3 - 3 M_{Jup} and 3 - 6 AU for Rowan et al. (2016).

To quantify this effect, we assume that planets in our sample are distributed according to a negative power law in mass, and a flat power law in semi-major axis. Specifically, we adopt the α value of -0.31 from Cumming et al. (2008), and a β value of 0. We choose not to adopt the Cumming et al power law coefficient for semi-major axis ($\beta = 0.26$), as this coefficient was derived from a fit to the population of gas giant planets inside 3 AU. This fit indicates that the frequency of these planets rises with increasing semi-major axis, but this is inconsistent with current constraints from both RV and direct imaging sur-

veys (Bryan et al. 2016; Bowler 2016; Clanton and Gaudi 2016; Bowler and Nielsen 2018), which prefer much flatter distributions at large semi-major axes. In Bryan et al. (2016) we found that for the population of gas giant planets with long-period companions, the occurrence rate of these companions decreases with increasing semi-major axis. While the current small sample size of directly imaged planets makes it difficult to determine their mass and semi-major axis distribution, their overall low occurrence rate indicates that a rising power law in semi-major axis is likely not applicable at wide separations.

For each of the nine systems with a statistically significant trend that do not have a resolved companion in this mass and semi-major axis range, we draw from the α = -0.31, β = 0 power law distribution until we have generated a sample of 100 simulated planets with a cutoff mass of 20 M_{Jup} that lie within the favored region of mass/semi-major axis parameter space where the probability of there existing a planet given the RV trend is greater than the probability of there being no planet given the RV trend. For each system we then count the fraction of planets that fall within the range $3-7$ AU and $0.3-13$ M_{Jup}. For the resolved companions, we count three companions that fall within this range and were thus included in the occurrence rate calculation. Averaging across all of the trend and resolved companion systems, we find that 61% of our simulated planet population lies inside this range. If we rescale our occurrence rate to account for the fact that $\sim$2/5 of our occurrence right might be attributed to companions outside the 3 - 7 AU semi-major axis range, we would then derive a corrected occurrence rate of $21\% \pm 4\%$ for our sample over this semi-major axis range. This reduced occurrence rate is still inconsistent with the Wittenmyer et al. value at the 3σ level.

We next consider results from other studies that provide independent estimates of the frequency of long period gas giant planets around nearby stars. Rowan et al. (2016) estimate the occurrence rate of Jupiter analogs using a sample of 1122 stars, where they define a Jupiter analog as a planet with a mass between $0.3-3$ M_{Jup} and semi-major axis between $3-6$ AU. As with Wittenmyer et al., they only consider planet detections with fully resolved orbits in their analysis. Over this range, they find an occurrence rate of $1-4\%$. While this integration range has a relatively strict mass limit, we note that previous power law fits to the population of RV-detected planets consistently indicate that lower mass gas giants are more common than higher mass gas giants (Cumming et al. 2008; Bryan et al. 2016), suggesting that their upper bound of 3 M_{Jup} versus our upper bound of 13 M_{Jup} is unlikely to change this integrated occurrence rate very much. We therefore conclude that our occurrence rate is likely higher than the rate from this study as well, with the same caveats as for the Wittenmyer et al. comparison.

For our last comparison we turn to Foreman-Mackey et al. (2016), who calculated the frequency of long period planets between $1.5-9$ AU and $0.01-20$ M_{Jup} using transit detections from the Kepler photometry. Unlike the previous two radial velocity studies, a majority of the long period planets in their sample have just one observed transit. Although this study is able to place some loose constraints on the orbital periods of these planets based on their measured transit durations, these constraints are nearly as broad as those for our radial velocity trend systems. For this parameter space Foreman-Mackey et al. (2016) find an occurrence rate density of 0.068 ± 0.019, corresponding to an integrated occurrence rate of $92.5\pm25.7\%$. Over a similar semi-major axis range and a more limited mass range ($1-10$ AU and $0.5-20$ M_{Jup}), we find an occurrence rate density of 0.045 ± 0.009 and an integrated occurrence rate of $38\pm7\%$. While these two occurrence rate densities are formally consistent, three-quarters of Foreman-Mackey et al. (2016)'s sample consists of planets whose estimated masses are less than 0.2 M_{Jup}, whereas all of our candidate companions have minimum masses higher than this threshold. We therefore conclude that there is relatively little overlap between the two planet samples, making this comparison less relevant than the studies by Wittenmyer et al. (2016) and Rowan et al. (2016).

4.3. *Implications of Our Results for Super-Earth Formation and Migration Models*

Although it is difficult to make quantitative comparisons without a better understanding of the power law distribution for the long period gas giant planets in our sample, our results indicate that there is a higher occurrence rate for gas giants in systems hosting inner super-Earths than for field stars. Furthermore, if we take our integrated occurrence rate of $34\pm7\%$ between $3-7$ AU and $0.3-13$ M_{Jup} at face value, as well as the overall occurrence rates of super-Earths and long-period gas giant planets (Howard et al. 2010; Fressin et al. 2013; Petigura et al. 2013; Wittenmyer et al. 2016; Rowan et al. 2016; Zhu et al. 2018), Equation 7 would suggest that a significant majority of long period gas giant planets have inner super-Earths.

4.3.1. *Long Period Gas Giants Do Not Hinder Super-Earth Formation, Did Not Migrate Large Distances*

The apparent correlation between the occurrence of inner super-Earths and outer gas giants suggests that gas giant companions do not hinder super-Earth formation, either by cutting off the flow of solids to the inner disk, stirring up the velocity distribution of these solids, or by preventing super-Earths formed at larger separations from migrating inward (Walsh et al. 2011; Batygin and Laughlin 2015; Moriarty and Fischer 2015; Izidoro et al. 2015). We also note that four of the super-Earth systems in our sample contain additional gas giant companions inside 1 AU, which were not included in our estimate of the frequency of exterior long period companions. These four inner gas giants are located immediately adjacent to and in some cases in between the super-Earths in these systems, providing additional support for the idea that the presence of gas giants does not disrupt super-Earth formation. It is likely that these inner gas giants with super-Earth companions did not undergo large scale migration: high eccentricity migration of any kind would destroy the orbits of inner planets (e.g. Mustill et al. 2015; Antonini et al. 2016), and disk-driven migration would lead to resonant locking among the giant planets and the super-Earths, resulting in a orbital architecture reminiscent of the Galilean satellites.

If the scenario for the solar system presented in Batygin and Laughlin (2015) is correct, this would also suggest

that the long-period gas giant companions in these systems did not undergo large-scale inward migration. A gas giant undergoing long-range migration (in Batygin and Laughlin 2015, Jupiter migrated from 6 AU to 1.5 AU) can capture solid materials in resonance, driving both the inward transport and the excitation of eccentricities. The ensuing collisional cascade among the resonant planetesimals shuttles newly formed super-Earths inward onto their host stars. In this scenario, the total mass participating in this cascade must be large enough to appreciably alter the orbital semi-major axes of inner super-Earths (i.e., it must have a total mass comparable to that of the planets). The amount of solids participating in cascade depends on the distance over which the outer gas giants migrates: $M_{\rm swarm} \sim f_{\rm solid} \times$ (nebula mass) $\times$ (migration distance / size of the disk)—where we assume a gas disk surface density profile of $\propto 1/r$ with r being the stellocentric distance, and $f_{\rm solid}$ is the solid-to-gas mass ratio. If, for example, the outer gas giant migrates only $\sim$1 AU for $f_{\rm solid} = 1/100$, nebula mass of $0.01 M_\odot$ and disk size of 30 AU, $M_{\rm swarm} \sim 1 M_\oplus$. This is not enough mass to shepherd inner super-Earths onto a host star, rendering this mechanism ineffective in systems where giant planets remain relatively close ($\sim$<1 AU) to their formation locations.

4.3.2. *Outer Gas Giants Provide Constraints on Protoplanetary Disk Properties*

We next consider whether or not the presence of an outer gas giant can be used to constrain the properties of the protoplanetary disks from which these systems formed. Large solid mass content is considered one such property, facilitating the growth of grains to planetesimals (e.g. Youdin and Chiang 2004; Birnstiel et al. 2012), accelerating the growth of cores by pebble accretion (e.g. Ormel and Kobayashi 2012; Lambrechts and Johansen 2014; Lin et al. 2018), and speeding up the final assembly by giant impact (e.g. Dawson et al. 2015).[6] Observationally, both gas giants and super-Earths (here defined as planets with mass of 1–10 $M_\oplus$ and/or with radii of 1–4 $R_\oplus$) are found to occur more frequently around metal-rich stars (Fischer and Valenti 2005; Petigura et al. 2018). Here we consider whether the metallicity of the host star—used as a proxy of the total solid content in the natal disk—is correlated with the occurrence of gas giant companions to inner super-Earths.

As a test of this question, we divide our sample into systems that have greater than 3σ trends and resolved companions ("Companion Systems") and those that do not ("No Companion Systems"), and compare the error weighted averages of the stellar metallicities between these two samples. For the transiting planet sample, we find average metallicities of 0.172±0.014 and 0.075±0.007 for the companion/no companion systems, a 5.9σ difference. For the RV sample, the average metallicities are 0.174±0.033 and -0.460±0.007 for the companion/no companion systems, a 19.0σ difference. However, at present the "no companion" RV sample error weighted average metallicity is significantly influenced by negative metallicities with small uncertainties for systems HD 20794 and HD 175607. We thus recalculate this error weighted average without these two systems, and find an error weighted average of -0.074±0.020, now a 6.5σ difference between the companion/no companion RV samples. We note that in this comparison we do not include M stars GJ 3293 and GJ 163. This is because we wanted to use metallicities for M stars derived using only IR techniques since they are consistent and calibrated on FGK stars, and neither of these M stars had metallicities derived using these techniques. These comparisons for the RV and transit samples suggest that super-Earth systems around metal-rich stars are more likely to have outer companions than their metal-poor counterparts. We plot the distribution of metallicities for companion/no companion systems for each sample in Figure 7. We note that the sample of stars in the RV sample typically have lower masses and correspondingly lower metallicities than stars in the transiting planet sample, with an error weighted average metallicity of -0.073±0.020 (without HD 20794 and HD 175607) and 0.103±0.007 for the RV and transiting samples respectively.

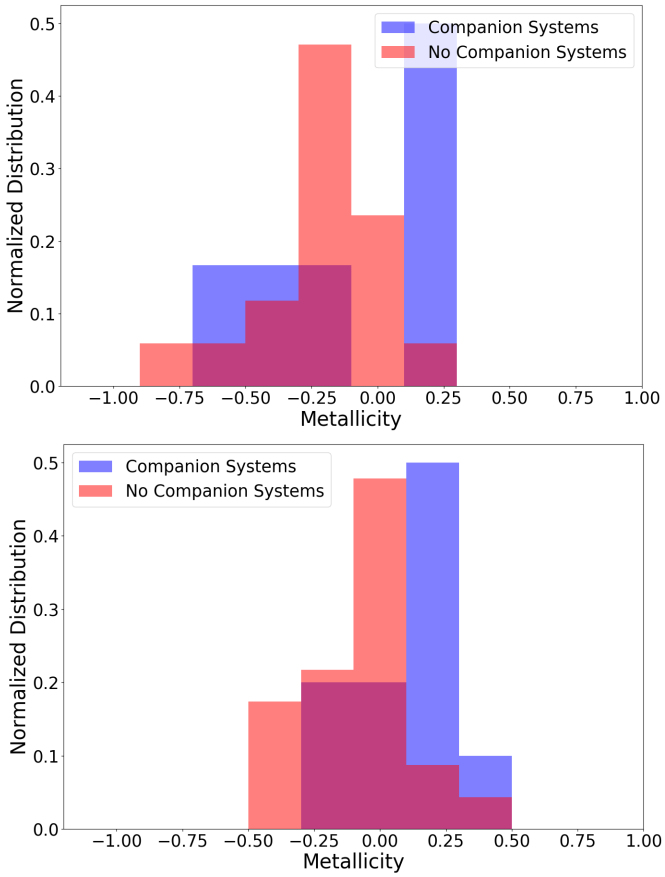

Figure 7. Distributions of stellar metallicities for systems with and without $> 3\sigma$ trends and resolved companions. Top: RV only sample. Bottom: Transit only sample.

We next consider whether or not there is any correlation between the presence of an outer gas giant companion and the mass of the host star. Observations of young stars indicate that disk mass appears to be correlated with stellar mass, albeit with large intrinsic vari-

[6] To be more precise, the growth of planetesimals and cores is governed by the "local" concentration of solids; in other words, what matters is the solid-to-gas mass ratio at the site of such growth, not necessarily the bulk mass ratio.

ance (Andrews et al. 2013; Pascucci et al. 2016). As with stellar metallicity, we expect that disks with higher overall masses will have a correspondingly higher surface density of solids. However, the benefits of this higher surface density for giant planet formation may be partially negated by the shorter average lifetimes of disks around more massive stars (Ribas et al. 2015). This might affect our estimates of the companion frequency in RV versus transiting planet systems, as these two samples have different stellar mass distributions. We find that while only one star in the transiting planet sample is an M dwarf (LHS 1140) out of 34 systems, ten targets are M dwarfs in the RV sample (out of 25). We calculate the occurrence rates for the combined RV and transiting planet sample without the M stars and with M stars only over an integration range of 0.5 – 20 M_{Jup} and 1 – 20 AU, and find occurrence rates of 37±8% and 44±17% respectively. This is consistent with the occurrence rate of the total sample of 39±7% to $< 0.1\sigma$.

5. CONCLUSIONS

We collected published RV data for a sample of 65 systems hosting at least one inner super-Earth planet in order to search for massive, long-period companions. We detect these distant companions as long term trends in the RV data when the orbital period of the companion is shorter than the system RV baseline. Out of our sample of 65 systems, we found 14 systems that had statistically significant trends. Two of these systems had resolved stellar companions that could potentially have caused the observed trends, while three more systems had trends that were likely due to stellar activity. We removed these five systems from subsequent analysis, leaving nine systems with statistically significant trends indicating the presence of an outer companion. Two of these trends are identified here for the first time, while seven were previously reported in the literature. We also identify 10 previously published resolved gas giant companions ($>$ 0.5 M_{Jup} and 1 – 20 AU) in our sample of systems. We report two new candidate planets in systems HD 156668 and HD 175607, but do not include these in our statistical study as they lie below our mass cutoff with minimum masses of 31 $M_\oplus$ and 24 $M_\oplus$ respectively. We also recover a fully resolved periodic signal in HD 1461 that appears to be caused by stellar activity, as reported in Bryan et al. (2016).

We compute 2D probability distributions in mass and semi-major axis space for each system in our sample with a radial velocity trend, where we use the duration and shape of the trends to place lower limits on allowed ranges of mass and separation. We use a combination of new and archival AO imaging at infrared wavelengths to place a corresponding upper limit on the allowed masses and separations of these companions. We find that the error-weighted average stellar metallicities of systems with gas giant companions are 5.9σ higher than those without companions for our transiting planet sample, and 6.5σ higher for our RV sample, in good agreement with the well-established metallicity correlation from RV surveys of field stars.

We fit the observed companion distributions with a double power law in mass and semi-major axis, and integrate this power law over 0.5 – 20 M_{Jup} and 1 – 20 AU to find an occurrence rate of 39 ± 7%. We then compare our occurrence rate for these companions to similar occurrence rates for long period gas giant planets from radial velocity surveys of sun-like field stars. We find that super-Earth systems appear to have more gas giant companions than we would expect to see by chance alone, even after accounting for the additional uncertainty introduced by our inability to pinpoint the precise locations of these companions for systems with radial velocity trends. The high occurrence rate of long period (>1 AU) gas giants in super-Earth systems in turn implies that a significant majority of the long period gas giants identified in radial velocity surveys of field stars likely host inner super-Earths. We therefore conclude that the presence of an outer gas giants does not hinder super-Earth formation, as proposed in some previous theoretical studies. To the contrary, our data suggest that these companions may either actively facilitate super-Earth formation or simply serve as a fossil record of early disk conditions that were particularly favorable for planet formation over a wide range of semi-major axes.

This work was supported by NSF CAREER grant 1555095, and was based in part on observations made at the W.M. Keck Observatory. We extend special thanks to those of Hawaiian ancestry on whose sacred mountain of Mauna Kea we are privileged to be guests. EJL is supported by the Sherman Fairchild Fellowship from Caltech.

REFERENCES

K. Tsiganis, R. Gomes, A. Morbidelli, and H. F. Levison, Nature **435**, 459 (2005).
S. N. Raymond, ApJ **643**, L131 (2006), astro-ph/0605136.
D. P. O'Brien, A. Morbidelli, and H. F. Levison, Icarus **184**, 39 (2006).
A. Morbidelli, J. I. Lunine, D. P. O'Brien, S. N. Raymond, and K. J. Walsh, Annual Review of Earth and Planetary Sciences **40**, 251 (2012), 1208.4694.
S. N. Raymond and A. Izidoro, Icarus **297**, 134 (2017), 1707.01234.
A. Morbidelli and A. Crida, Icarus **191**, 158 (2007).
M. Lambrechts, A. Johansen, and A. Morbidelli, A&A **572**, A35 (2014), 1408.6087.
A. Morbidelli, B. Bitsch, A. Crida, M. Gounelle, T. Guillot, S. Jacobson, A. Johansen, M. Lambrechts, and E. Lega, Icarus **267**, 368 (2016), 1511.06556.
S. J. Desch, A. Kalyaan, and C. M. O. Alexander, ArXiv e-prints (2017), 1710.03809.
K. J. Walsh, A. Morbidelli, S. N. Raymond, D. P. O'Brien, and A. M. Mandell, in *Lunar and Planetary Science Conference* (2011), vol. 42 of *Lunar and Planetary Inst. Technical Report*, p. 2585.
K. Batygin and G. Laughlin, Proceedings of the National Academy of Science **112**, 4214 (2015), 1503.06945.
D. N. C. Lin and J. Papaloizou, ApJ **309**, 846 (1986).
A. Crida, A. Morbidelli, and F. Masset, Icarus **181**, 587 (2006), astro-ph/0511082.
W. Kley and R. P. Nelson, ARA&A **50**, 211 (2012), 1203.1184.
J. Moriarty and D. Fischer, ApJ **809**, 94 (2015), 1507.08215.
F. L. Whipple, in *From Plasma to Planet*, edited by A. Elvius (1972), p. 211.
F. S. Masset, A. Morbidelli, A. Crida, and J. Ferreira, ApJ **642**, 478 (2006).
W. K. M. Rice, P. J. Armitage, K. Wood, and G. Lodato, MNRAS **373**, 1619 (2006), astro-ph/0609808.
Y. Hasegawa and R. E. Pudritz, MNRAS **417**, 1236 (2011), 1105.4015.
A. Morbidelli and D. Nesvorny, A&A **546**, A18 (2012), 1208.4687.

T. Sato, S. Okuzumi, and S. Ida, A&A **589**, A15 (2016), 1512.02414.
J. Wallace, S. Tremaine, and J. Chambers, AJ **154**, 175 (2017), 1705.08932.
B. M. S. Hansen, MNRAS **467**, 1531 (2017), 1608.06300.
B. Pu and D. Lai, MNRAS (2018), 1801.06220.
C. X. Huang, C. Petrovich, and E. Deibert, AJ **153** (2017).
A. Izidoro, S. N. Raymond, A. Morbidelli, F. Hersant, and A. Pierens, ApJ **800**, L22 (2015), 1501.06308.
J. B. Pollack, O. Hubickyj, P. Bodenheimer, J. J. Lissauer, M. Podolak, and Y. Greenzweig, Icarus **124**, 62 (1996).
D. A. Fischer and J. Valenti, ApJ **622**, 1102 (2005).
J. A. Johnson, K. M. Aller, A. W. Howard, and J. R. Crepp, PASP **122**, 905 (2010), 1005.3084.
R. I. Dawson, E. Chiang, and E. J. Lee, MNRAS **453**, 1471 (2015), 1506.06867.
C. Yasui, N. Kobayashi, A. T. Tokunaga, M. Saito, and C. Tokoku, ApJ **723**, L113 (2010), 1010.1668.
B. Ercolano and C. J. Clarke, MNRAS **402**, 2735 (2010), 0910.5110.
L. A. Buchhave, M. Bizzarro, D. W. Latham, D. Sasselov, W. D. Cochran, M. Endl, H. Isaacson, D. Juncher, and G. W. Marcy, Nature **509**, 593 (2014), 1405.7695.
E. A. Petigura, G. W. Marcy, J. N. Winn, L. M. Weiss, B. J. Fulton, A. W. Howard, E. Sinukoff, H. Isaacson, T. D. Morton, and J. A. Johnson, AJ **155**, 89 (2018), 1712.04042.
A. Cumming, R. P. Butler, G. W. Marcy, S. S. Vogt, J. T. Wright, and D. A. Fischer, PASP **120**, 531 (2008), 0803.3357.
A. W. Howard, G. W. Marcy, J. A. Johnson, D. A. Fischer, J. T. Wright, H. Isaacson, J. A. Valenti, J. Anderson, D. N. C. Lin, and S. Ida, Science **330**, 653 (2010), 1011.0143.
M. Mayor, M. Marmier, C. Lovis, S. Udry, D. Ségransan, F. Pepe, W. Benz, J. . Bertaux, F. Bouchy, X. Dumusque, et al., ArXiv e-prints (2011), 1109.2497.
C. D. Dressing and D. Charbonneau, ApJ **807**, 45 (2015), 1501.01623.
M. L. Bryan, H. A. Knutson, A. W. Howard, H. Ngo, K. Batygin, J. R. Crepp, B. J. Fulton, S. Hinkley, H. Isaacson, J. A. Johnson, et al., ApJ **821**, 89 (2016), 1601.07595.
D. Rowan, S. Meschiari, G. Laughlin, S. S. Vogt, R. P. Butler, J. Burt, S. Wang, B. Holden, R. Hanson, P. Arriagada, et al., ApJ **817**, 104 (2016), 1512.00417.
R. A. Wittenmyer, R. P. Butler, C. G. Tinney, J. Horner, B. D. Carter, D. J. Wright, H. R. A. Jones, J. Bailey, and S. J. O'Toole, ApJ **819**, 28 (2016), 1601.05465.
G. W. Marcy, H. Isaacson, A. W. Howard, J. F. Rowe, J. M. Jenkins, S. T. Bryson, D. W. Latham, S. B. Howell, T. N. Gautier, III, N. M. Batalha, et al., ApJS **210**, 20 (2014), 1401.4195.
L. M. Weiss and G. W. Marcy, ApJ **783**, L6 (2014), 1312.0936.
C. D. Dressing, D. Charbonneau, X. Dumusque, S. Gettel, F. Pepe, A. Collier Cameron, D. W. Latham, E. Molinari, S. Udry, L. Affer, et al., ApJ **800**, 135 (2015), 1412.8687.
N. Astudillo-Defru, T. Forveille, X. Bonfils, D. Ségransan, F. Bouchy, X. Delfosse, C. Lovis, M. Mayor, F. Murgas, F. Pepe, et al., A&A **602**, A88 (2017), 1703.05386.
S. Uehara, H. Kawahara, K. Masuda, S. Yamada, and M. Aizawa, ApJ **822**, 2 (2016), 1602.07848.
D. Foreman-Mackey, T. D. Morton, D. W. Hogg, E. Agol, and B. Schölkopf, AJ **152**, 206 (2016), 1607.08237.
B. T. Montet, J. R. Crepp, J. A. Johnson, A. W. Howard, and G. W. Marcy, ApJ **781**, 28 (2014), 1307.5849.
H. A. Knutson, B. J. Fulton, B. T. Montet, M. Kao, H. Ngo, A. W. Howard, J. R. Crepp, S. Hinkley, G. Á. Bakos, K. Batygin, et al., ApJ **785**, 126 (2014), 1312.2954.
F. Fressin, G. Torres, D. Charbonneau, S. T. Bryson, J. Christiansen, C. D. Dressing, J. M. Jenkins, L. M. Walkowicz, and N. M. Batalha, ApJ **766**, 81 (2013), 1301.0842.
E. A. Petigura, A. W. Howard, and G. W. Marcy, Proceedings of the National Academy of Science **110**, 19273 (2013), 1311.6806.
W. Zhu, C. Petrovich, Y. Wu, S. Dong, and J. Xie, ArXiv e-prints (2018), 1802.09526.
M. López-Morales, R. D. Haywood, J. L. Coughlin, L. Zeng, L. A. Buchhave, H. A. C. Giles, L. Affer, A. S. Bonomo, D. Charbonneau, A. Collier Cameron, et al., AJ **152**, 204 (2016), 1609.07617.
S. B. Howell, J. F. Rowe, S. T. Bryson, S. N. Quinn, G. W. Marcy, H. Isaacson, D. R. Ciardi, W. J. Chaplin, T. S. Metcalfe, M. J. P. F. G. Monteiro, et al., ApJ **746**, 123 (2012), 1112.2165.
W. J. Borucki, D. G. Koch, N. Batalha, S. T. Bryson, J. Rowe, F. Fressin, G. Torres, D. A. Caldwell, J. Christensen-Dalsgaard, W. D. Cochran, et al., ApJ **745**, 120 (2012), 1112.1640.
J. A. Dittmann, J. M. Irwin, D. Charbonneau, X. Bonfils, N. Astudillo-Defru, R. D. Haywood, Z. K. Berta-Thompson, E. R. Newton, J. E. Rodriguez, J. G. Winters, et al., Nature **544**, 333 (2017), 1704.05556.
Z. K. Berta-Thompson, J. Irwin, D. Charbonneau, E. R. Newton, J. A. Dittmann, N. Astudillo-Defru, X. Bonfils, M. Gillon, E. Jehin, A. A. Stark, et al., Nature **527**, 204 (2015), 1511.03550.
X. Dumusque, A. S. Bonomo, R. D. Haywood, L. Malavolta, D. Ségransan, L. A. Buchhave, A. Collier Cameron, D. W. Latham, E. Molinari, F. Pepe, et al., ApJ **789**, 154 (2014), 1405.7881.
D. Queloz, F. Bouchy, C. Moutou, A. Hatzes, G. Hébrard, R. Alonso, M. Auvergne, A. Baglin, M. Barbieri, P. Barge, et al., A&A **506**, 303 (2009).
R. Alonso, C. Moutou, M. Endl, J.-M. Almenara, E. W. Guenther, M. Deleuil, A. Hatzes, S. Aigrain, M. Auvergne, A. Baglin, et al., A&A **567**, A112 (2014), 1406.1270.
S. Gettel, D. Charbonneau, C. D. Dressing, L. A. Buchhave, X. Dumusque, A. Vanderburg, A. S. Bonomo, L. Malavolta, F. Pepe, A. Collier Cameron, et al., ApJ **816**, 95 (2016), 1511.09097.
J. M. Almenara, N. Astudillo-Defru, X. Bonfils, T. Forveille, A. Santerne, S. Albrecht, S. C. C. Barros, F. Bouchy, X. Delfosse, O. Demangeon, et al., A&A **581**, L7 (2015), 1509.02917.
T. N. Gautier, III, D. Charbonneau, J. F. Rowe, G. W. Marcy, H. Isaacson, G. Torres, F. Fressin, L. A. Rogers, J.-M. Désert, L. A. Buchhave, et al., ApJ **749**, 15 (2012), 1112.4514.
E. A. Petigura, E. Sinukoff, E. D. Lopez, I. J. M. Crossfield, A. W. Howard, J. M. Brewer, B. J. Fulton, H. T. Isaacson, D. R. Ciardi, S. B. Howell, et al., AJ **153**, 142 (2017a), 1702.00013.
W. J. Borucki, E. Agol, F. Fressin, L. Kaltenegger, J. Rowe, H. Isaacson, D. Fischer, N. Batalha, J. J. Lissauer, G. W. Marcy, et al., Science **340**, 587 (2013), 1304.7387.
M. Endl, P. Robertson, W. D. Cochran, P. J. MacQueen, E. J. Brugamyer, C. Caldwell, R. A. Wittenmyer, S. I. Barnes, and K. Gullikson, ApJ **759**, 19 (2012), 1208.5709.
B. E. Nelson, E. B. Ford, J. T. Wright, D. A. Fischer, K. von Braun, A. W. Howard, M. J. Payne, and S. Dindar, MNRAS **441**, 442 (2014), 1402.6343.
S. S. Vogt, R. A. Wittenmyer, R. P. Butler, S. O'Toole, G. W. Henry, E. J. Rivera, S. Meschiari, G. Laughlin, C. G. Tinney, H. R. A. Jones, et al., ApJ **708**, 1366 (2010), 0912.2599.
R. P. Butler, S. S. Vogt, G. Laughlin, J. A. Burt, E. J. Rivera, M. Tuomi, J. Teske, P. Arriagada, M. Diaz, B. Holden, et al., AJ **153**, 208 (2017), 1702.03571.
A. W. Howard, G. W. Marcy, D. A. Fischer, H. Isaacson, P. S. Muirhead, G. W. Henry, T. S. Boyajian, K. von Braun, J. C. Becker, J. T. Wright, et al., ApJ **794**, 51 (2014), 1408.5645.
T. Forveille, X. Bonfils, X. Delfosse, M. Gillon, S. Udry, F. Bouchy, C. Lovis, M. Mayor, F. Pepe, C. Perrier, et al., A&A **493**, 645 (2009), 0809.0750.
X. Delfosse, X. Bonfils, T. Forveille, S. Udry, M. Mayor, F. Bouchy, M. Gillon, C. Lovis, V. Neves, F. Pepe, et al., A&A **553**, A8 (2013), 1202.2467.
A. Suárez Mascareño, J. I. González Hernández, R. Rebolo, N. Astudillo-Defru, X. Bonfils, F. Bouchy, X. Delfosse, T. Forveille, C. Lovis, M. Mayor, et al., A&A **597**, A108 (2017), 1611.02122.
M. Mayor, X. Bonfils, T. Forveille, X. Delfosse, S. Udry, J.-L. Bertaux, H. Beust, F. Bouchy, C. Lovis, F. Pepe, et al., A&A **507**, 487 (2009), 0906.2780.
G. Anglada-Escudé, M. Tuomi, E. Gerlach, R. Barnes, R. Heller, J. S. Jenkins, S. Wende, S. S. Vogt, R. P. Butler, A. Reiners, et al., A&A **556**, A126 (2013), 1306.6074.

G. Anglada-Escudé, P. Arriagada, S. S. Vogt, E. J. Rivera, R. P. Butler, J. D. Crane, S. A. Shectman, I. B. Thompson, D. Minniti, N. Haghighipour, et al., ApJ **751**, L16 (2012), 1202.0446.
N. Astudillo-Defru, X. Bonfils, X. Delfosse, D. Ségransan, T. Forveille, F. Bouchy, M. Gillon, C. Lovis, M. Mayor, V. Neves, et al., A&A **575**, A119 (2015), 1411.7048.
G. Lo Curto, M. Mayor, W. Benz, F. Bouchy, C. Lovis, C. Moutou, D. Naef, F. Pepe, D. Queloz, N. C. Santos, et al., A&A **512**, A48 (2010).
F. Pepe, C. Lovis, D. Ségransan, W. Benz, F. Bouchy, X. Dumusque, M. Mayor, D. Queloz, N. C. Santos, and S. Udry, A&A **534**, A58 (2011), 1108.3447.
R. A. Wittenmyer, M. Tuomi, R. P. Butler, H. R. A. Jones, G. Anglada-Escudé, J. Horner, C. G. Tinney, J. P. Marshall, B. D. Carter, J. Bailey, et al., ApJ **791**, 114 (2014), 1406.5587.
F. Bouchy, M. Mayor, C. Lovis, S. Udry, W. Benz, J.-L. Bertaux, X. Delfosse, C. Mordasini, F. Pepe, D. Queloz, et al., A&A **496**, 527 (2009), 0812.1608.
B. J. Fulton, L. M. Weiss, E. Sinukoff, H. Isaacson, A. W. Howard, G. W. Marcy, G. W. Henry, B. P. Holden, and R. I. Kibrick, ApJ **805**, 175 (2015), 1504.06629.
R. F. Diaz, D. Segransan, S. Udry, C. Lovis, F. Pepe, X. Dumusque, M. Marmier, R. Alonso, W. Benz, F. Bouchy, et al., A&A **585**, A134 (2016), 1510.06446.
G. Anglada-Escudé, P. J. Amado, J. Barnes, Z. M. Berdiñas, R. P. Butler, G. A. L. Coleman, I. de La Cueva, S. Dreizler, M. Endl, B. Giesers, et al., Nature **536**, 437 (2016), 1609.03449.
J. L. Christiansen, A. Vanderburg, J. Burt, B. J. Fulton, K. Batygin, B. Benneke, J. M. Brewer, D. Charbonneau, D. R. Ciardi, A. Collier Cameron, et al., AJ **154**, 122 (2017), 1706.01892.
L. Affer, G. Micela, M. Damasso, M. Perger, I. Ribas, A. Suárez Mascareño, J. I. González Hernández, R. Rebolo, E. Poretti, J. Maldonado, et al., A&A **593**, A117 (2016), 1607.03632.
A. C. M. Correia, J. Couetdic, J. Laskar, X. Bonfils, M. Mayor, J.-L. Bertaux, F. Bouchy, X. Delfosse, T. Forveille, C. Lovis, et al., A&A **511**, A21 (2010), 1001.4774.
A. Mortier, J. P. Faria, N. C. Santos, V. Rajpaul, P. Figueira, I. Boisse, A. Collier Cameron, X. Dumusque, G. Lo Curto, C. Lovis, et al., A&A **585**, A135 (2016), 1511.03941.
X. Bonfils, G. Lo Curto, A. C. M. Correia, J. Laskar, S. Udry, X. Delfosse, T. Forveille, N. Astudillo-Defru, W. Benz, F. Bouchy, et al., A&A **556**, A110 (2013), 1306.0904.
M. Gillon, B.-O. Demory, V. Van Grootel, F. Motalebi, C. Lovis, A. C. Cameron, D. Charbonneau, D. Latham, E. Molinari, F. A. Pepe, et al., Nature Astronomy **1**, 0056 (2017), 1703.01430.
X. Bonfils, M. Gillon, T. Forveille, X. Delfosse, D. Deming, B.-O. Demory, C. Lovis, M. Mayor, V. Neves, C. Perrier, et al., A&A **528**, A111 (2011), 1102.1420.
J. Sahlmann, P. F. Lazorenko, D. Ségransan, N. Astudillo-Defru, X. Bonfils, X. Delfosse, T. Forveille, J. Hagelberg, G. Lo Curto, F. Pepe, et al., A&A **595**, A77 (2016), 1608.00918.
E. Sinukoff, A. W. Howard, E. A. Petigura, B. J. Fulton, H. Isaacson, L. M. Weiss, J. M. Brewer, B. M. S. Hansen, L. Hirsch, J. L. Christiansen, et al., AJ **153**, 70 (2017), 1612.04851.
M. Neveu-VanMalle, D. Queloz, D. R. Anderson, D. J. A. Brown, A. Collier Cameron, L. Delrez, R. F. Díaz, M. Gillon, C. Hellier, E. Jehin, et al., A&A **586**, A93 (2016), 1509.07750.
F. Dai, J. N. Winn, P. Arriagada, R. P. Butler, J. D. Crane, J. A. Johnson, S. A. Shectman, J. K. Teske, I. B. Thompson, A. Vanderburg, et al., ApJ **813**, L9 (2015), 1510.03811.
E. A. Petigura, A. W. Howard, G. W. Marcy, J. A. Johnson, H. Isaacson, P. A. Cargile, L. Hebb, B. J. Fulton, L. M. Weiss, T. D. Morton, et al., AJ **154**, 107 (2017b), 1703.10400.
A. Léger, D. Rouan, J. Schneider, P. Barge, M. Fridlund, B. Samuel, M. Ollivier, E. Guenther, M. Deleuil, H. J. Deeg, et al., A&A **506**, 287 (2009), 0908.0241.
X. Bonfils, X. Delfosse, S. Udry, N. C. Santos, T. Forveille, and D. Ségransan, A&A **442**, 635 (2005), astro-ph/0503260.
K. C. Schlaufman and G. Laughlin, A&A **519**, A105 (2010), 1006.2850.
A. W. Howard, J. A. Johnson, G. W. Marcy, D. A. Fischer, J. T. Wright, G. W. Henry, H. Isaacson, J. A. Valenti, J. Anderson, and N. E. Piskunov, ApJ **726**, 73 (2011), 1003.3444.
B. Rojas-Ayala, K. R. Covey, P. S. Muirhead, and J. P. Lloyd, ApJ **748**, 93 (2012), 1112.4567.
G. Cayrel de Strobel, C. Soubiran, and N. Ralite, A&A **373**, 159 (2001), astro-ph/0106438.
L. Zhao, D. A. Fischer, J. Brewer, M. Giguere, and B. Rojas-Ayala, AJ **155**, 24 (2018), 1711.06320.
D. A. Fischer, G. W. Marcy, and J. F. P. Spronck, ApJS **210**, 5 (2014), 1310.7315.
B. J. Fulton, E. A. Petigura, S. Blunt, and E. Sinukoff, PASP **130**, 044504 (2018), 1801.01947.
S. S. Vogt, R. P. Butler, G. W. Marcy, D. A. Fischer, G. W. Henry, G. Laughlin, J. T. Wright, and J. A. Johnson, ApJ **632**, 638 (2005).
R. E. Kass and A. E. Raftery, Journal of the American Statistical Association **90**, 773 (1995), https://amstat.tandfonline.com/doi/pdf/10.1080/01621459.1995.10476572, URL `https://amstat.tandfonline.com/doi/abs/10.1080/01621459.1995.10476572`.
K. G. Stassun, K. A. Collins, and B. S. Gaudi, AJ **153**, 136 (2017), 1609.04389.
A. M. Tanner, C. R. Gelino, and N. M. Law, PASP **122**, 1195 (2010), 1007.4315.
D. R. Rodriguez, G. Duchêne, H. Tom, G. M. Kennedy, B. Matthews, J. Greaves, and H. Butner, MNRAS **449**, 3160 (2015), 1503.01320.
E. Furlan, D. R. Ciardi, M. E. Everett, M. Saylors, J. K. Teske, E. P. Horch, S. B. Howell, G. T. van Belle, L. A. Hirsch, T. N. Gautier, III, et al., AJ **153**, 71 (2017), 1612.02392.
H. Ngo, H. A. Knutson, M. L. Bryan, S. Blunt, E. L. Nielsen, K. Batygin, B. P. Bowler, J. R. Crepp, S. Hinkley, A. W. Howard, et al., AJ **153**, 242 (2017), 1704.02326.
R. Lenzen, M. Hartung, W. Brandner, G. Finger, N. N. Hubin, F. Lacombe, A.-M. Lagrange, M. D. Lehnert, A. F. M. Moorwood, and D. Mouillet, in *Instrument Design and Performance for Optical/Infrared Ground-based Telescopes*, edited by M. Iye and A. F. M. Moorwood (2003), vol. 4841 of *Proc. SPIE*, pp. 944–952.
G. Rousset, F. Lacombe, P. Puget, N. N. Hubin, E. Gendron, T. Fusco, R. Arsenault, J. Charton, P. Feautrier, P. Gigan, et al., in *Adaptive Optical System Technologies II*, edited by P. L. Wizinowich and D. Bonaccini (2003), vol. 4839 of *Proc. SPIE*, pp. 140–149.
T. Meshkat, M. A. Kenworthy, S. P. Quanz, and A. Amara, ApJ **780**, 17 (2014), 1310.8577.
H. Ngo, H. A. Knutson, S. Hinkley, J. R. Crepp, E. B. Bechter, K. Batygin, A. W. Howard, J. A. Johnson, T. D. Morton, and P. S. Muirhead, ApJ **800**, 138 (2015), 1501.00013.
M. Service, J. R. Lu, R. Campbell, B. N. Sitarski, A. M. Ghez, and J. Anderson, PASP **128**, 095004 (2016).
I. Baraffe, G. Chabrier, F. Allard, and P. H. Hauschildt, A&A **337**, 403 (1998), astro-ph/9805009.
G. Torres, PASP **111**, 169 (1999).
M. C. Liu, D. A. Fischer, J. R. Graham, J. P. Lloyd, G. W. Marcy, and R. P. Butler, ApJ **571**, 519 (2002), astro-ph/0112407.
Gaia Collaboration, T. Prusti, J. H. J. de Bruijne, A. G. A. Brown, A. Vallenari, C. Babusiaux, C. A. L. Bailer-Jones, U. Bastian, M. Biermann, D. W. Evans, et al., A&A **595**, A1 (2016a), 1609.04153.
Gaia Collaboration, A. G. A. Brown, A. Vallenari, T. Prusti, J. H. J. de Bruijne, F. Mignard, R. Drimmel, C. Babusiaux, C. A. L. Bailer-Jones, U. Bastian, et al., A&A **595**, A2 (2016b), 1609.04172.
J. T. Wright, G. W. Marcy, R. P. Butler, and S. S. Vogt, ApJS **152**, 261 (2004), astro-ph/0402582.
H. Isaacson and D. Fischer, ApJ **725**, 875 (2010), 1009.2301.
G. Anglada-Escudé and M. Tuomi, A&A **548**, A58 (2012), 1206.7118.
D. M. Kipping, MNRAS **434**, L51 (2013), 1306.4982.
S. Tabachnik and S. Tremaine, MNRAS **335**, 151 (2002), astro-ph/0107482.
B. P. Bowler, J. A. Johnson, G. W. Marcy, G. W. Henry, K. M. G. Peek, D. A. Fischer, K. I. Clubb, M. C. Liu, S. Reffert, C. Schwab, et al., ApJ **709**, 396 (2010), 0912.0518.
W. Zhu and Y. Wu, ArXiv e-prints (2018), 1805.02660.
B. P. Bowler, PASP **128**, 102001 (2016), 1605.02731.
C. Clanton and B. S. Gaudi, ApJ **819**, 125 (2016), 1508.04434.

B. P. Bowler and E. L. Nielsen, ArXiv e-prints arXiv:1802.10132 (2018), 1802.10132.
A. J. Mustill, M. B. Davies, and A. Johansen, ApJ **808**, 14 (2015), 1502.06971.
F. Antonini, A. S. Hamers, and Y. Lithwick, AJ **152**, 174 (2016), 1604.01781.
A. N. Youdin and E. I. Chiang, ApJ **601**, 1109 (2004), astro-ph/0309247.
T. Birnstiel, H. Klahr, and B. Ercolano, A&A **539**, A148 (2012), 1201.5781.
C. W. Ormel and H. Kobayashi, ApJ **747**, 115 (2012), 1112.0274.
M. Lambrechts and A. Johansen, A&A **572**, A107 (2014), 1408.6094.
J. W. Lin, E. J. Lee, and E. Chiang, ArXiv e-prints (2018), 1806.00487.
S. M. Andrews, K. A. Rosenfeld, A. L. Kraus, and D. J. Wilner, ApJ **771**, 129 (2013), 1305.5262.
I. Pascucci, L. Testi, G. J. Herczeg, F. Long, C. F. Manara, N. Hendler, G. D. Mulders, S. Krijt, F. Ciesla, T. Henning, et al., ApJ **831**, 125 (2016), 1608.03621.
Á. Ribas, H. Bouy, and B. Merín, A&A **576**, A52 (2015).